HUMAN LOCALIZATION AND ACTIVITY RECOGNITION USING DISTRIBUTED MOTION SENSORS

By

DHARMENDRA CHANDRASHEKAR KALLUR

Bachelor of Engineering in Electronics and Communication

Visvesvaraya Technological University

Belgaum, Karnataka

2010

Submitted to the Faculty of the
Graduate College of the
Oklahoma State University
in partial fulfillment of
the requirements for
the Degree of
MASTER OF SCIENCE
July, 2014

HUMAN LOCALIZATION AND ACTIVITY RECOGNITION USING DISTRIBUTED MOTION SENSORS

Thesis Approved:

Dr. Weihua Sheng

Thesis Adviser

Dr. Qi Cheng

Dr. Rama Ramakumar

.

ACKNOWLEDGEMENTS

I would like to express my sincere gratitude to Professor Dr. Weihua Sheng for his support, guidance, patience and motivation. He has been a great advisor and mentor throughout my Master's program.

Besides my advisor I would like to thank my other committee members: Dr. Qi Cheng and Dr. Rama Ramakumar who gave me insightful comments and valuable feedback.

My deepest gratitude goes to my parents Chandrashekar Kallur, Bharathi Hosamane and my sister Kusuma Chandrashekar for their encouragement and support.

I would like to thank my fellow research assistants Duy Tran, Jianhao Du, Minh Pham and Dan Yang for their help, useful comments and constructive suggestions.

I would also like to express my gratitude to all my friends Ahmed Basheer, Praveen Batapati, Vasumathi Chalasani, Arun Dhanapal, Shweta Gavai, Sandeep Hosangadi, Megha Kumsi, Zeel Maheshwari, Rajashekargouda Patil, Ravish Shetty and Neeharika Thunga for their enormous help, constant encouragement and moral support.

Acknowledgements reflect the views of the author and are not endorsed by committee members or Oklahoma State University.

Name: DHARMENDRA CHANDRASHEKAR KALLUR

Date of Degree: JULY, 2014

Title of Study: MASTER OF SCIENCE

Major Field: ELECTRICAL ENGINEERING

Abstract: The purpose of this thesis is to localize a human and recognize his/her activities in indoor environments using distributed motion sensors. We propose to use a test bed simulated as mock apartment for conducting our experiments. The two parts of the thesis are localization and activity recognition of the elderly person. We explain complete hardware and software setup used to provide these services. The hardware setup consists of two types of sensor end nodes and two sink nodes. The two types of end nodes are Passive Infrared sensor node and GridEye sensor node. Passive Infrared sensor nodes consist of Passive Infrared sensors for motion detection. GridEye sensor nodes consist of thermal array sensors. Data from these sensors are acquired using Arduino boards and transmitted using Xbee modules to the sink nodes. The sink nodes consist of receiver Xbee modules connected to a computer. The sensor nodes were strategically placed at different place inside the apartment. The thermal array sensor provides 64 pixel temperature values, while the PIR sensor provides binary information about motion in its field of view. Since the thermal array sensor provides more information, they were placed in large rooms such as living room and bed room. While PIR sensors were placed in kitchen and bathroom. Initially GridEye sensors are calibrated to obtain the transformation between pixel and real world coordinates. Data from these sensors were processed on computer and we were able to localize the human inside the apartment. We compared the location accuracy using ground truth data obtained from the OptiTrack system. GridEye sensors were also used for activity recognition. Basic human activities such as sitting, sleeping, standing and walking were recognized. We used Support Vector Machine (SVM) to recognize sitting and sleeping activities. Gait speed of human was used to recognize the standing and walking activities. Experiments were performed to obtain the accuracy of classification for these activities.

TABLE OF CONTENTS

Chapter Page

LIST OF TABLES

Table Page

LIST OF FIGURES

Figure Page

Figure Page

CHAPTER I

1. INTRODUCTION

Rapidly increasing population of elderly people gives us a lot of opportunities and challenges. This chapter explains the motivation behind our thesis research. This chapter also provides the overall approach of thesis and an overview of remaining chapters in this thesis.

1.1 Motivation

The world population is ageing rapidly. The elderly population had increased to almost 810 million in 2012. And in 2050, the number of aged people (60 and above) is about to reach a staggering 2 billion. Between 2000 and 2050, proportion of the world's population over 60 years will double from about 11% to 22%. This is an increase from 605 million to 2 billion over the same period [1][2].

Elderly people are an important asset to society. The life experience and wisdom they have gained over the years make them a vital social resource. However, along with these benefits there are added challenges. Providing older people with “age-friendly” physical and social environments helps them live an independent fuller life and also improves the active participation, maximizing their contribution to the society [2].

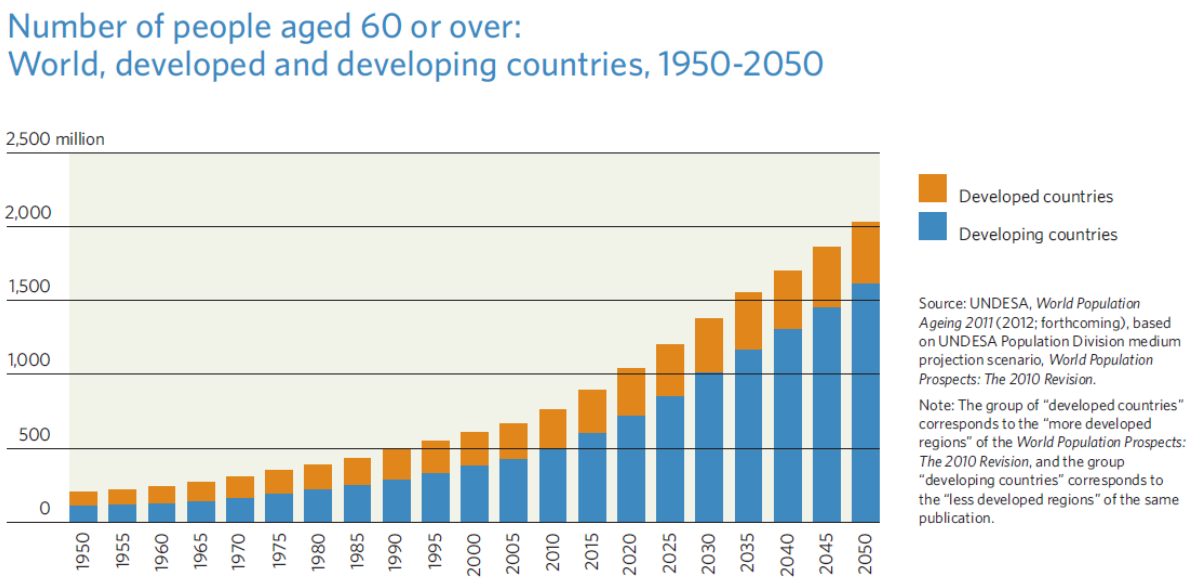

Figure 1.1 Graph of people aged 60 or above [2].

We live in a busy world. It's becoming hard for people to take care of elderly at home. It is difficult for people to monitor elderly by staying at home due to hectic work life. Elders have the option of going to adult day care, long term care, nursing homes, hospice care, and home care. Even though all these options support the health, nutritional, social support, and daily living needs of adults, the feeling of independence is lost. Elders would prefer to stay in the comfort of their home where they feel more confident than moving to any expensive adult care or healthcare facility. Hence if older adult is able to complete self-care activities on their own, encouraging them in their efforts in maintaining independence can provide them with a sense of accomplishment and ability to maintain independence longer [3]. The best way to support them is to provide a physical environment that promotes the development and use of innovative technologies that encourage active ageing [2]. Home automation that provides security, entertainment, and energy conservation and tailored to the elderly would be the perfect use of technology to achieve this. A smart home along with a domestic robot can be used to keep a caring eye on the elderly [4][5]. The main objective in order to accomplish any of these tasks would require us to localize the elderly first. Real-time indoor monitoring plays an important role

in living assistance, emergency detection, surveillance of target and many more location based services. These types of location based services are very helpful for elderly in their daily lives. GPS (Global Positioning System) plays an important role in localization. But since GPS signal weakens inside the building, it cannot be used for indoor environment [6]. We have to overcome this disability with alternate technology. Numerous terminal and non-terminal based approaches exist that are used to track the human indoor. Terminal based approaches include RFID tags to be carried along with the person to be tracked. Non – terminal based approach include use of ultra sound, Pyroelectric Infrared sensors, smart floors or cameras to track the human. There are some disadvantages associated with Terminal based approach: the subject has to carry the device with him/her all the time. This would be great discomfort to the user. Also if the device is not carried by them, then it is impossible to track using this method. Smart floor falls short in maintenance [7]. With non-terminal based method, various sensors are distributed within the home that helps in tracking human. Cameras are more accurate. But, certainly, cameras breach privacy and therefore are not preferred in day-to-day life. We could use distributed PIR sensors to locate the human but PIR sensors have their own advantages and disadvantages. PIR sensors have to be placed throughout the home and also a lot of these have to be used in order to have high degree of accuracy. In this thesis we are using a fusion of infrared array sensors and PIR sensors to locate the elderly. The infrared array sensors used in this thesis are developed using thermopile technology and is similar to an Infrared camera but of very low resolution. The resolution is good enough to locate a human but not high enough to detect the face of the person. Hence it is a perfect fit for an application such as indoor localization. These sensors along with PIR sensors in specific locations help in localizing the human.

The infrared array sensor can also be used to detect the daily activities of the elderly at home. By training the system to detect these activities and can be used to analyze the pattern of living. All these data also give the elderly's children or relatives to keep a caring eye on them and their

activities and to check if they are safe. This system can also help detect fire and also intrusion alert when no one is at home.

1.2 Contributions

The overall thesis is divided into two parts. First is the localization of the elderly person and second is the activity recognition of the elderly person.

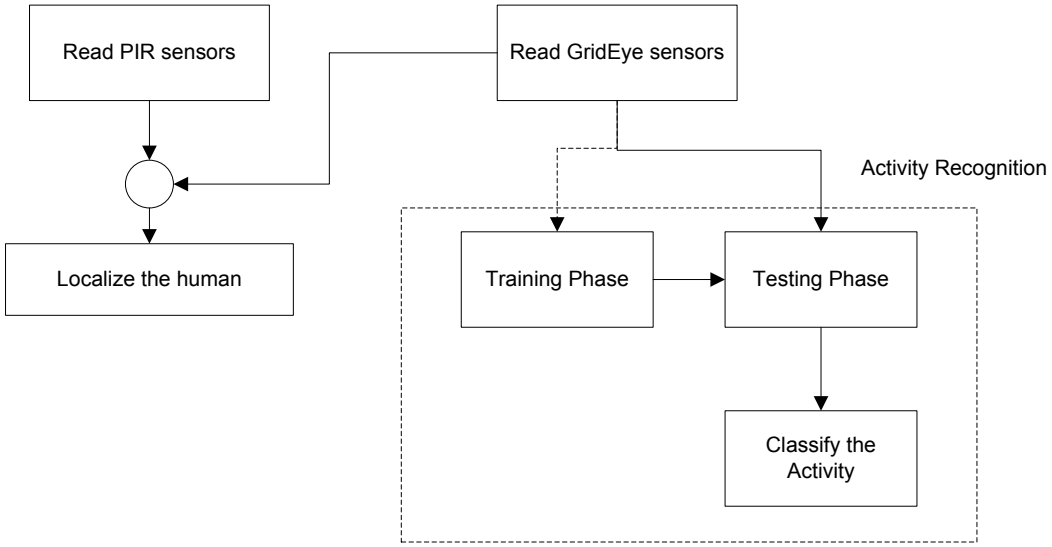

Figure 1.2 Overall approach

The overall approach of this research is shown in Figure 1.2. There are two kinds of sensors used in this thesis. One is the PIR sensor which is a Passive Infrared Sensor. This is a binary sensor whose digital output is either one or zero. Whenever the sensor detects a motion it outputs a one and when there is no motion it outputs a zero. The other sensor is an infrared array sensor is an 8x8 thermopile array sensor. This sensor gives temperature values of each of the 64 pixels. Both these sensors are strategically placed inside the apartment to locate the elderly. Due to the high accuracy of the IR array sensor, they are placed in larger living spaces such as living room, family rooms and bed rooms. While the binary PIR sensors are placed in smaller spaces such as kitchen and bathroom. In the first part of the thesis the combination of these two sensors is used

to localize the elderly. Data from multiple of these sensors is collected to a central processing station when the data is analyzed. The data acquisition is done by wireless Xbee devices. The sensors are connected to end nodes. Here raw data is collected from each of the sensor and then transmitted through the Xbee devices using Zigbee protocol.

In the second part of the thesis we identify the activity of the elderly using data collected from the thermopile array sensor. Since the array sensor is more like a low resolution IR camera, the heat signature of each activity can be used to first train the system and then using this model we can identify the human activity. Here we use the SVM supervised learning model to identify the activity. Initially each of the activity that has to be identified is trained to the system with an appropriate label. Later the SVM classifies the real time data and identifies the activity according to the trained model.

1.3 Thesis Overview

A brief overview of various chapters in remainder of the thesis is as follows.

Chapter II presents a review of literature work related to home automation, localization and activity recognition, respectively.

Chapter III describes about sensors and sensor node used in our system. This includes an explanation about Passive Infrared sensor node and thermal array sensor node. The hardware and software description of each of these nodes is provided in this chapter. This chapter also describes the test bed used to conduct our experiments.

Chapter IV explains the calibration process conducted to transform pixel coordinates to real world coordinates.

Chapter V provides a description of the human localization method. It also explains about Kalman filter used in this method. A brief explanation about the method used to measure accuracy is also provided.

Chapter VI describes activity recognition algorithm used in this thesis.

Chapter VII provides a description of various experiments performed and results obtained.

Chapter VIII presents the conclusion of our experimental findings. Scope for future work is also provided in this chapter.

CHAPTER II

2. RELATED WORK

Increase in life expectancy and higher-quality lives are few factors that have led to increase in the population of elderly people in the world. This is a blessing because of the amount of experience and knowledge they bring to the society. But along with this they offer us lot of challenges to face in order to provide a more supportive environment for them. Due to these reasons, Gerontechnology is gaining importance in recent times.

"Gerontechnology is the study of the interaction between technology and the unique challenges and needs of older people faced with limited physical or cognitive abilities." [8].

A lot of research is going on in developing smart homes, social robots, assistive technology and telemedicine. A wide range of software, wearable devices and personal assistance devices are being developed to help assist the elderly [8].

This chapter explains research in the field of home automation, indoor localization and activity recognition.

2.1 Home Automation

Aware Home Research Initiative (AHRI) at Georgia Institute of Technology has constructed a three-story, 5,040 square-feet house to address the social challenges faced by people at home. One of the major challenges researched is the design of smart home to help the elderly people. In this research facility, the location of human is identified using RF ID tags. Each person wears a passive RFID tag below the knee. Antennas in the form of floor mats are distributed throughout the house that can track the IDs on the person.

This system provides room level occupancy accuracy. To improve accuracy and to recognize the human activity, a series of unobtrusive cameras are installed on the first floor of the Aware Home. By using location, gestures and interaction with other objects the behavior of the human is recognized. [9].

Gator Tech Smart House in The University of Florida has similar research to help the aged and disabled people. Gator Tech Smart House is fitted with various smart devices to help day to day activities of the occupant. Ultrasonic transceivers are placed in each room and the user has to wear a vest with an ultrasonic tag. The location of the resident is detected using triangulation. These help in detecting occupant's movements, location and orientation. Smart floors are used to track the location of occupants. They are also used to detect occupants fall. Smart cameras are used for video surveillance and motion detection. Smart phone operate as traditional telephone and is also used to operate various gadgets at home. Smart thermostats are used to personalize air conditioning and heat settings throughout house [10].

In [11], Mrazovac et al., developed software based home control system to automatically control the audio and video devices in Smart home. They use visual 3D camera, microphone and passive infrared sensors to detect and localize the human. These sensors sense the behavioral patterns of human. Based on these patterns various home appliances were controlled.

Extensive research for elder care is carried out at Center for Eldercare and Rehabilitation Technology (CERT) center at Missouri University [12]. Sensor networks have been installed in an apartment. Various sensors used include motion sensor, chair pads, stove sensor and bed sensor. Data collected from these devices is studies and intelligent algorithm extract patterns of activity to detect health change. Vision sensors, depth sensors, acoustic arrays and radar are used to detect human fall. Gait parameters were collected and analyzed to detect risk of fall. The sensor network also includes a passive hydraulic bed sensor. This sensor captures quantitative pulse and respiration rates. This information was used to detect illness well in advance.

2.2 Indoor Localization

In all the above home automation research the foremost important objective is to locate the human inside home. There are many techniques used to localize the resident. The three major techniques are Triangulation, Proximity and Scene analysis [13]. Since GPS does not work well in indoor locations, alternative techniques like Active Badge and Active Bat are used. Active Badge was developed at Olivetti Research Laboratory and it uses diffuse infrared technology. Each person has to carry a small infrared badge. The badge emits a unique signal every 15 seconds or on demand which was collected by central server [14]. Active Bat developed by AT&T uses ultrasonic location system to locate the resident using the principle of trilateration. The Bat (Transmitter) emitted a short pulse of ultrasound signal to the receivers mounted at known points on the ceiling. Using the time of flight of the pulse, distance of the Bat from each receiver was calculated and the 3D position of the Bat was determined [15].

Cricket is another example that uses the ultrasound technology to localize the human. Cricket indoor location system consists of location beacons and listeners. Beacons are transmitters that are attached to the ceiling of buildings and receivers called listeners are attached to devices that

require location information. Active beacons transmit location information and an ultrasonic pulse. The passive listener captures this information to calculate its distance from the beacon [16].

To locate human more accurately Easy Living uses two sets of stereo color cameras for tracking multiple humans [17]. Even though this method provides a practical person-tracking system, privacy of the person is lost.

In [18], Yu et al., used multiple cameras and floor sensors to localize the human in a Smart home environment. The system consisted of three components such as Camera Localization, Sensory Floor Localization and Condensation Tracker. The presence of the person was detected by the sensory floor by measuring the pressure variation. The cameras detected the person by using background subtraction and human template matching. The localization by both the floor sensors and the cameras was done separately. The Condensation Tracker was used to improve accuracy of localization. The failure of some sensors was overcome by fusing the data from multiple sensors.

Lately, Pyroelectric Infrared Sensors are being used to detect and localize human because of its simplicity. In [19], Hsiao et al., proposed a method to detect and localize the human inside home using pyroelectric infrared sensor networks. In this paper a combination of multiple PIR were installed on the ceiling. The procedure has initial offline training where a unique identifying set matched for each of the location regions is saved as a fingerprint. Using this fingerprint database as a lookup table, the identifying set from the online testing phase is mapped. By this method the target location is recognized. The room where the human needs to be detected was divided into a grid of 1m wide. The sensor was placed on the ceiling of the room and the identifying code at each grid point was determined and recorded into the database. Later during online testing phase when a human was at a particular grid point, he triggered an identifying code which when compared to the lookup table gave the location of human.

In [20], Lee et al., proposed a technique to track the path of the human movement indoor using the pyroelectric infrared sensor. An array of PIR sensors were placed in a room such that the sensing areas of two or more sensors overlap. The experiment was conducted on a test bed. A total of 12 sensors were placed such that maximum overlap of sensing area occurs and also such that all of the test bed was covered. A sensor placement was finally considered with 28 sensing areas covering the entire test bed. They have conducted several experiments to localize the human and track his trajectory. A location accuracy of 0.5m was achieved by the system.

PIR sensors are simple binary sensors that have both an advantage and a disadvantage. The advantage of being binary is that less processing time is required. But the disadvantage is that very less information is received. When a person is still in the area of interest, then the sensor gives a false negative. Also in all these research on localization of the human, in order to have an accurate result many sensors had to be placed throughout the home in strategic places. Installing many sensors causes increase of purchase cost and maintenance cost.

With the advancement in MEMS technology, many small format thermal infrared sensors are being developed. These sensors use the thermopile technology to generate digital temperature data from these thermopile outputs [21]. These sensors have advantage over binary PIR sensors and optical cameras. Despite providing more information than the binary sensors, they still do not breach the privacy of the person unlike the regular camera. Hence these sensors are great instruments to be used in home automation projects.

Erickson et al., in [22] proposed a Thermal Occupancy Sensing System (TOSS) using a thermopile array sensor. The main objective of this system was to determine the occupancy of a particular zone within a building in order to provide it to a building's energy management system. The system consisted of a combination of a PIR sensor and a thermopile array sensor - GridEye. The PIR sensor detected occupancy, while the IR array sensor was used to detect number of

occupants. The system initially took a background reading when the room was not occupied. Using this background the subsequent reads were subtracted. By doing this they could get the active components where the temperature was more than a standard deviation over the mean. The Connected Components were used over these active components and a feature vector was created with the total number of active quadrants, total number of connected components and the largest component. This feature vector was later passed to K-Nearest Neighbors to determine the occupancy count.

2.3 Activity Recognition

Activity recognition plays an important role in assisting elderly people and monitoring human activities anomalies. Research papers related to activity recognition are presented below.

Current research employ several approaches for activity recognition such as, wearable sensor based, vision sensor based, depth sensor based, distributed motion sensor based etc.

Bao et al., [23] recognized activities of human using wearable sensors. They developed an algorithm to detect physical activities from data acquired from five biaxial accelerometers. These accelerometers were worn on different parts of the body. Accelerometer data was collected from various subjects performing different activities. Decision tree classifier classified the mean energy, frequency-domain entropy and correlation of acceleration data. Walking, sitting, standing still, watching TV and various other activities were recognized by analyzing the data collected from these sensors.

In [24], Zang et al., used vision and depth based sensors for recognizing human activity. They proposed using four dimensional local spatio-temporal features for activity recognition. 4-dimensional local spatio-temporal feature includes intensity and depth information collected from 3D camera. Feature points were extracted by applying separate filters along the 3D spatial dimensions and 1D temporal dimension. Latent Dirichlet Allocation with Gibbs sampling was

used as the classifier to recognize human activities. Six types of human activities such as lifting, removing, pushing, waving, walking and signaling were recognized using the proposed method.

Activity recognition explained in [23] requires the user to wear a device. While in [24], the privacy of the user is at risk. A system that overcomes these two issues was developed by Okada et al., in [25]

In [25] Okada et al., used the thermopile array sensor to understand the daily activities of Visually Impaired Persons instead of using a convectional optical camera which would invade the privacy of the person. The system consisted of a Grid-Eye sensor connected to an Arduino Uno. The data read from the sensor was saved into a microSD card for further processing. The various behavior patterns were determined using the SVM. Initially the data from the sensor was saved to the microSD card. A video of the activity was also taken so that the activity could be labeled accordingly using the timestamps from both. Later by using trained SVM the activities of visually impaired person were determined. Since each activity produced different temperature distributions, various activities such as sitting on a chair, sitting on floor, standing were recognized.

In [26], Gonzalez et al., proposed a system to recognize energy-related activities in offices using thermopile sensors. A GridEye sensor was placed in an office building pantry area to recognize the activities in that area. The sensor was used and each of the pixel temperature was compared to the ambient temperature to determine the occupancy of the pixel. The pixels were classified into stationary objects and dynamic objects. A set of 21 activities involving the interaction between these stationary and dynamic objects was scripted. Using the classifiers, the state and interaction classes were determined. SVM was used as the classifier and was trained using the dataset. Using this real life study, dataset was evaluated and classified.

In this work, both the PIR sensors and thermopile array sensors will be used to locate the human inside the home and thermopile array sensor was used to recognize the human's activity. The experiments were conducted in a mock apartment.

CHAPTER III

3. SENSOR PLATFORM

Passive Infrared sensors nodes and thermal array sensors nodes are used to localize the human and recognize activity of the human. This chapter provides a description of these sensor nodes. It also explains the test bed used in our experiments.

3.1 Passive Infrared Sensor Node

Passive Infrared sensors (PIR sensors) are sensors that detect the IR radiations emitted by the objects that generate heat. The sensor in the device is split into two parts such that they detect the change in the radiation caused by motion in its field of view. The changes in the amount of IR radiation on the element, changes the voltage generated. This is fed to an on-board amplifier that processes the signal and provides it to the output pin [27].

The Figure 3.1 shows how the PIR sensor produces an output when it detects movement from objects radiating IR rays. When a human passes the field of view of the PIR sensor, the heat generated by the human body causes the PIR sensor to produce an output. The output is generated because of the change in the IR radiations received by the PIR sensor. This can be seen in Figure 3.2. The PIR sensor is usually capped with a Fresnel lens. A Fresnel lens is a plano convex lens that is used to condense the outside light into the sensor.

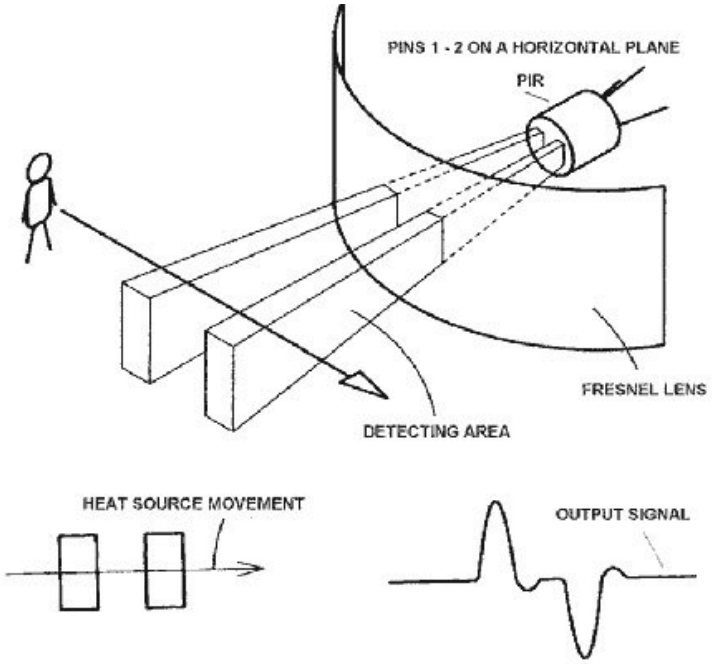

Figure 3.1PIR sensor working [28].

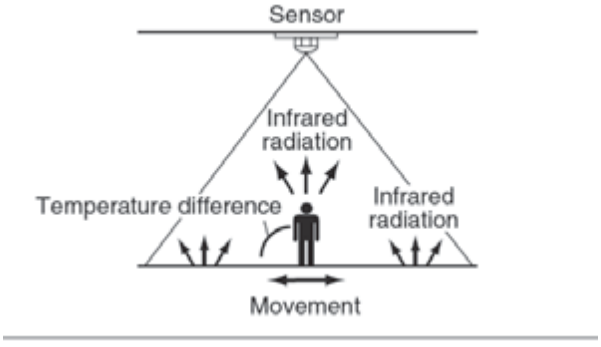

Figure 3.2 Passive Infrared Motion sensor working [29].

The PIR sensor used in this project was Panasonic EKMC1601111. The device specifications are shown in Table 3.1.

Parameter	Details
Rated consumption current	170μA
Rated operating voltage	3.0VDC – 6.0VDC
Output current (When detecting)	100μA
Output Voltage (When detecting)	Vdd – 0.5VDC min
Circuit Stability time	30s max
Detection distance	5m
Detection range (Horizontal x Vertical)	94° x 82°
Detection zone	64 zones

Table 3.1 Panasonic EKMC1601111 specification [30]

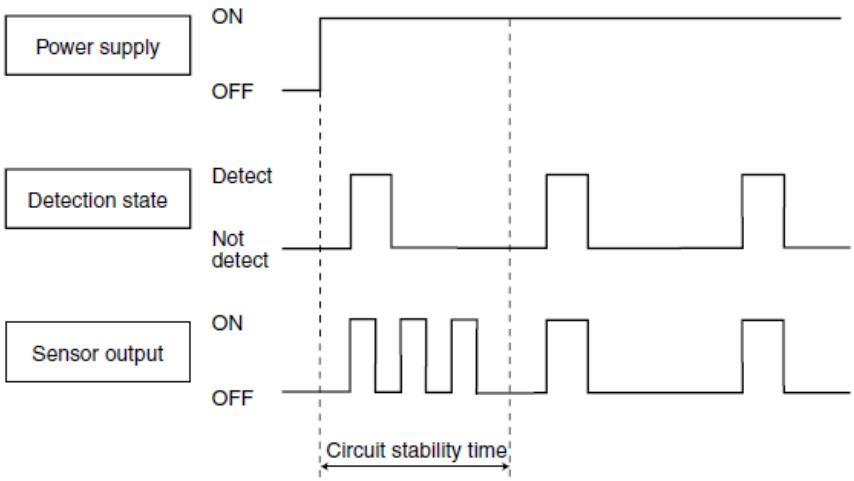

Figure 3.3 Timing diagram of PIR sensor [30].

The timing chart for the sensor is shown in Figure 3.3. The sensor produces a digital high whenever a movement is detected. There is a stability time of 30sec when the sensor is powered up. The output of the sensor is not stable during this startup time.

3.1.1 Hardware Setup

The PIR Sensor node consists of the following hardware parts.

- Arduino Mega 2560
- Panasonic PIR sensor
- 10k ohm resistor
- 2 LEDs
- Xbee shield
- Xbee module

The Arduino Mega 2560 is the brain of the sensor node which is a microcontroller board based on the ATmega2560. It has 54 digital input/output pins (of which 14 can be used as PWM outputs), 16 analog inputs, 4 UARTs (hardware serial ports), a 16 MHz crystal oscillator, a USB connection, a power jack, an ICSP header, and a reset button. An XBee shield along with an Xbee module is placed on the Arduino board. The Xbee module is used to transmit the sensor data wirelessly to the gateway node.

The PIR sensor was built into a circuit board with a pull-down resistor to the output pin. This ensures that false positives are not encountered.

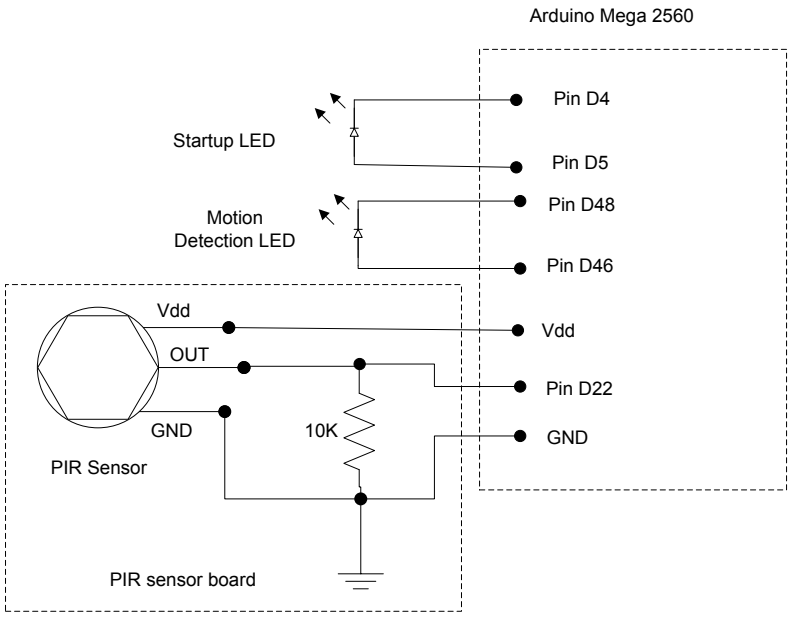

Figure 3.4 Circuit diagram of PIR sensor node

Figure 3.4 is the circuit diagram of the PIR sensor board. The PIR sensor board consists of the PIR sensor, the pull down resistor and the pin outs VDD, OUT and GND to the Arduino Mega 2560 board. The Startup LED is turned on when the sensor node is powered up for the first time. The Motion detection LED is turned on wherever the sensor detects motion in its field of view. Since the sensor has a very large field of view, it is restricted by attaching a cylindrical structure around it. By doing this we could change the sensor area by increasing or decreasing the height of the cylinder.

Figure 3.5 is the picture of PIR sensor node. The PIR circuit board is fixed to the Arduino board. The Xbee shield along with the Xbee module is fitted to the Arduino board. Two LEDs are used to indicate the sensor start up and motion detection. A cylindrical structure is fitted outside the PIR sensor to vary the field of view.

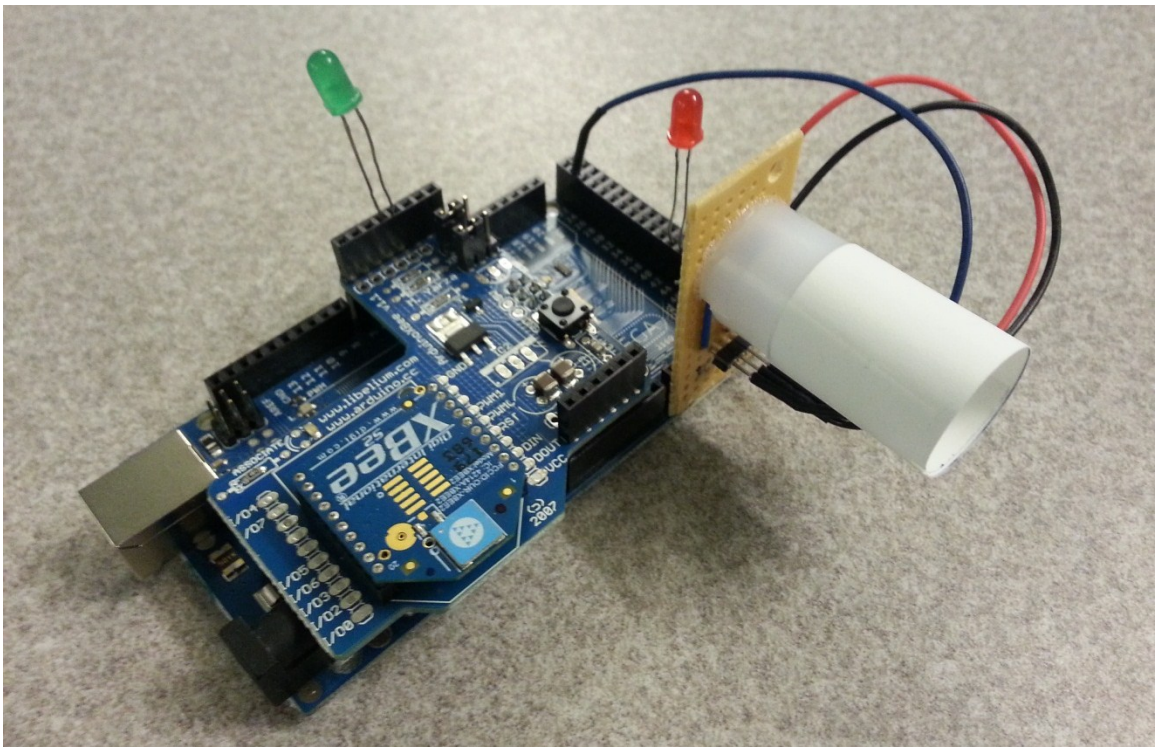

Figure 3.5 Picture of PIR sensor node

3.1.2 Software

The Arduino is programmed using Arduino IDE. The firmware on the Arduino reads the sensor and transmits it to the gateway node through the Xbee module. On startup all the I/O ports are initialized and the startup LED is turned on for 30 sec. During startup time the sensor is not read since the output is not stable. After the startup time the senor is read continuously. When the sensor detects motion, the sensor outputs a digital high and an encoded data is transmitted through the Xbee module. The encoded data contains the sensor ID and the status of the motion.

When the motion stops, the sensor outputs a low and another encoded data is transmitted to gateway node. A person is considered to be in the sensor's field of view after the start of motion byte is transmitted and before the stop of motion byte is transmitted. The sensor outputs a high when an object enters its field of view. But the sensor outputs a high even when the object moves

out of the sensor area. This alternating signal can be considered as though the subject has moved out of the field of view and entered again. Hence a low pass filter is introduced in the firmware code so that these two signals can be considered as a single motion activity. Figure 3.6 is the flowchart of firmware downloaded into Arduino of PIR sensor node.

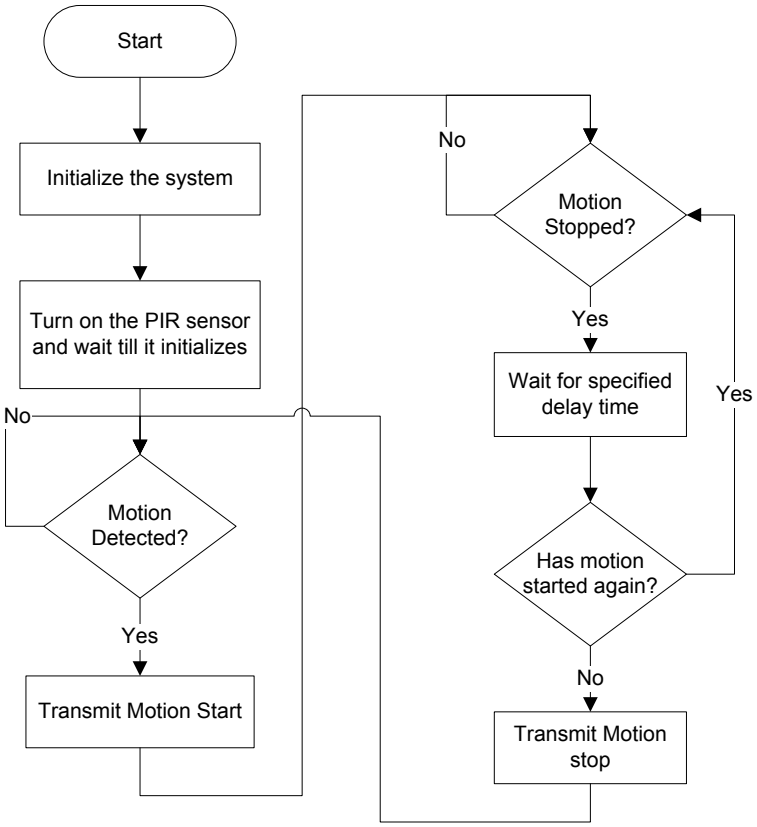

Figure 3.6 Flowchart of PIR sensor node firmware

3.2 Thermopile Array Sensor Node

A thermopile is an electronic device that converts thermal energy into electrical energy. A thermopile consists of a number of thermocouple junction pairs connected electrically in either series or parallel. When one of the thermocouple junctions absorbs thermal radiation, its temperature increases. This junction is called an active junction. The temperature difference between the active junction and the reference junction kept at a fixed temperature produces an electromotive force. Seebeck effect is the principle that is responsible for the generation of voltage in a thermopile. According to the Seebeck effect the voltage produced is proportional to the temperature difference between the two junctions [31][32].

We are using a MEMS based Panasonic Infrared array sensor Grid-EYE (AMG8831). Grid-EYE is a thermopile array sensor that features 64 thermopile elements in an 8x8 grid format. This sensor consists of a built-in thermistor and an integrated circuit is used to measure actual temperature. Each of the 64 thermopile elements has a 7.5° field of view and the sensor has a 60° viewing angle. Grid-EYE uses I2C communication interface [27].

The specification of the sensor is given in Table 3.2.

Item	Ratings
Applied Voltage	3.3V±0.3V
Temperature range of measuring object	0°C to 80°C +32°F to +176°F
Temperature accuracy	Typical ±2.5°C ±4.5°F
Detection distance	Max. 5m 16.404ft
Viewing angle	Typical 60°
Setup time	Typical 50ms (Time to enable communication after

	setup) Typical 15s (Time to stabilize output after setup)
Frame rate	Typical 10 frames/sec
Temperature output resolution	0.25°C
Thermistor output resolution	0.0625°C

Table 3.2 GridEye sensor specifications [33]

3.2.1 Hardware Setup

The Grid-EYE sensor node consists of the following hardware parts:

- Grid-EYE sensor board
- Arduino Mega 2560
- Xbee shield
- Xbee module

GridEye sensor board consists of 4 wire connector Vdd, GND, SDA and SCL. The connections between the GridEye sensor board and the Arduino board are shown in the Figure 3.5.

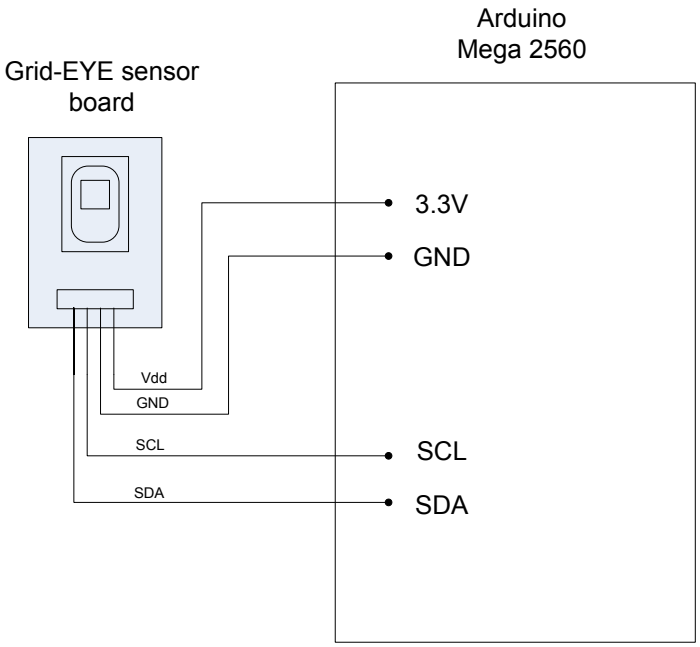

Figure 3.7 GridEye sensor node circuit diagram

The Arduino board also has an Xbee shield and an XBee module to transmit the data from the GridEye sensor to the gateway node.

3.2.2 Software

The Arduino board, to which the GridEye sensor was connected, was programmed using Arduino IDE. The firmware on the Arduino board reads the GridEye sensor data and transmits it to the gateway node through the Xbee module. The GridEye sensor is read using I2C protocol. The sensor provides 2 bytes for each of 64 pixels in the 8x8 grid. It also provides two byte thermistor value, which is the ambient temperature. After a frame is read from the GridEye sensor, it is transmitted to the gateway node serially using the Xbee module.

Figure 3.6 is the flowchart of the firmware downloaded onto the Arduino of GridEye sensor node.

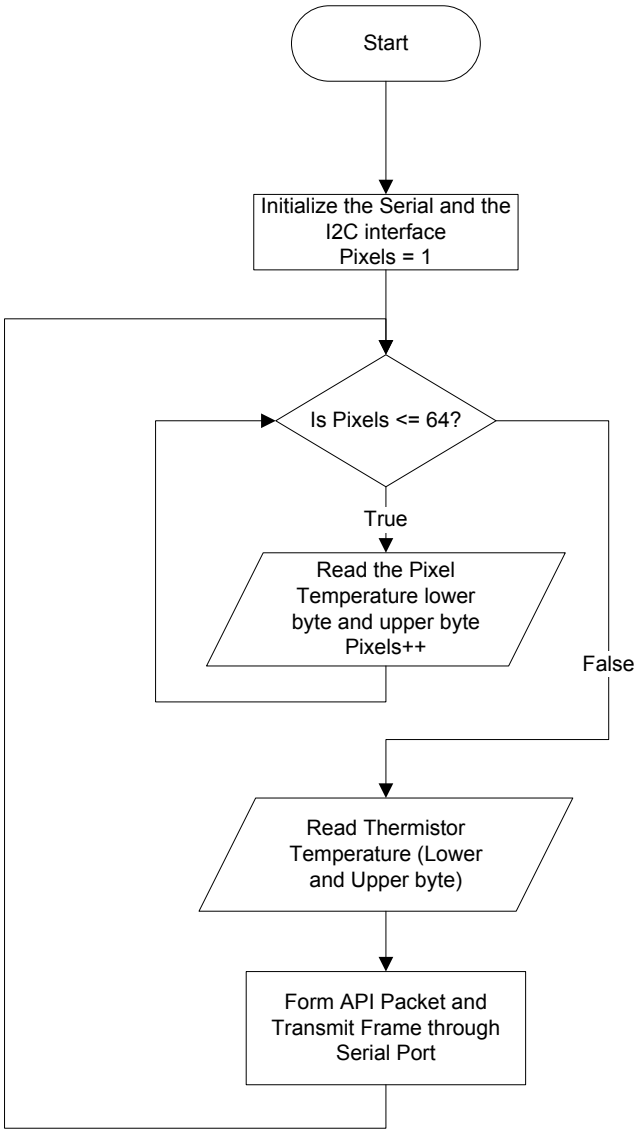

Figure 3.8 Flowchart of firmware on GridEye node

In order to transmit the frame through the Xbee module, a packet was formed which was compliant with API mode. By using the Xbee module in API mode we have the advantage to separate the frames from multiple GridEye sensors at the gateway.

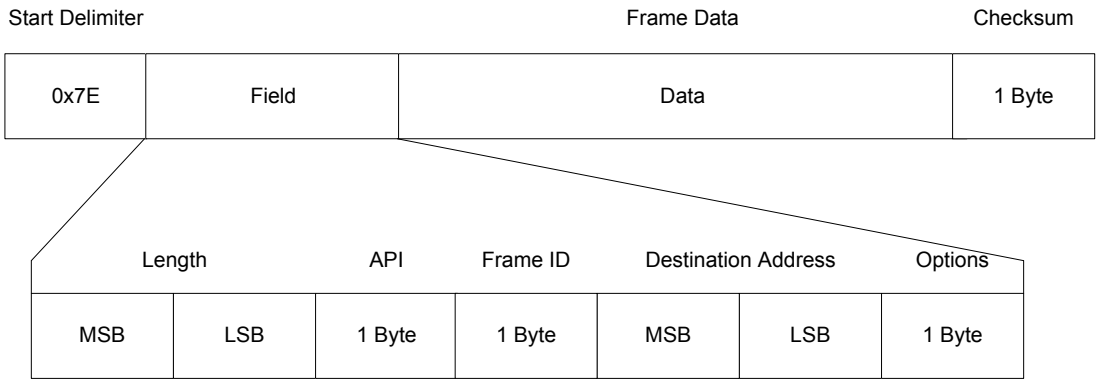

Figure 3.9 Xbee API packet

Field Name	**Field Value**	**Description**
Delimiter	0x7E	Start Delimiter
Length	2 bytes	Number of bytes between length and checksum fields.
API	0x01	Tx16 Request
Frame ID	0x00	No response is requested
Destination Address	2 bytes	Destination 16-bit network address
Options	0x00	Retry transmission if failed
Data	Variable	Up to 100 bytes of payload.
Checksum	1 byte	0xFF minus 8-bit sum of bytes between the length and checksum fields.

Table 3.3 Xbee API packet description

The API mode packet format is shown in Figure 3.7. The packet starts with a Start Delimiter. The Length, API identifier, Frame ID, Destination Address, Options follows the Start Delimiter. Data up to 100 bytes can be sent as payload. The Checksum is the last byte of the packet. The description of each field in the API packet is explained in Table 3.3.

Since only 100 bytes of payload can be sent in one packet, two API packets for each frame of sensor were sent. Each pixel in the frame is of 2 bytes. The first 32 pixels of the frame were transmitted in the first API packet. The second API packet consisted of the remaining 32 pixels

and the thermistor temperature. The flowchart of the firmware on the Arduino board is shown in Figure 3.8.

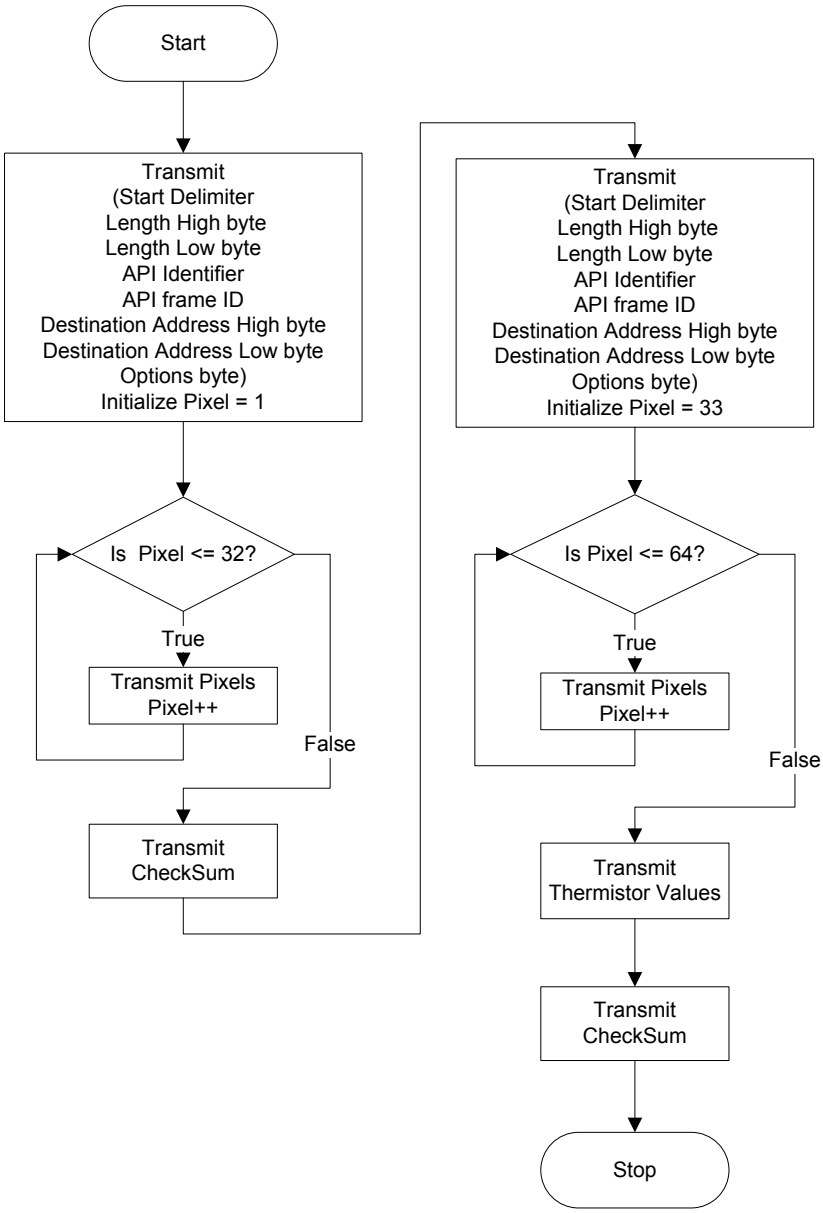

Figure 3.10 Flowchart of Xbee API packet transmission

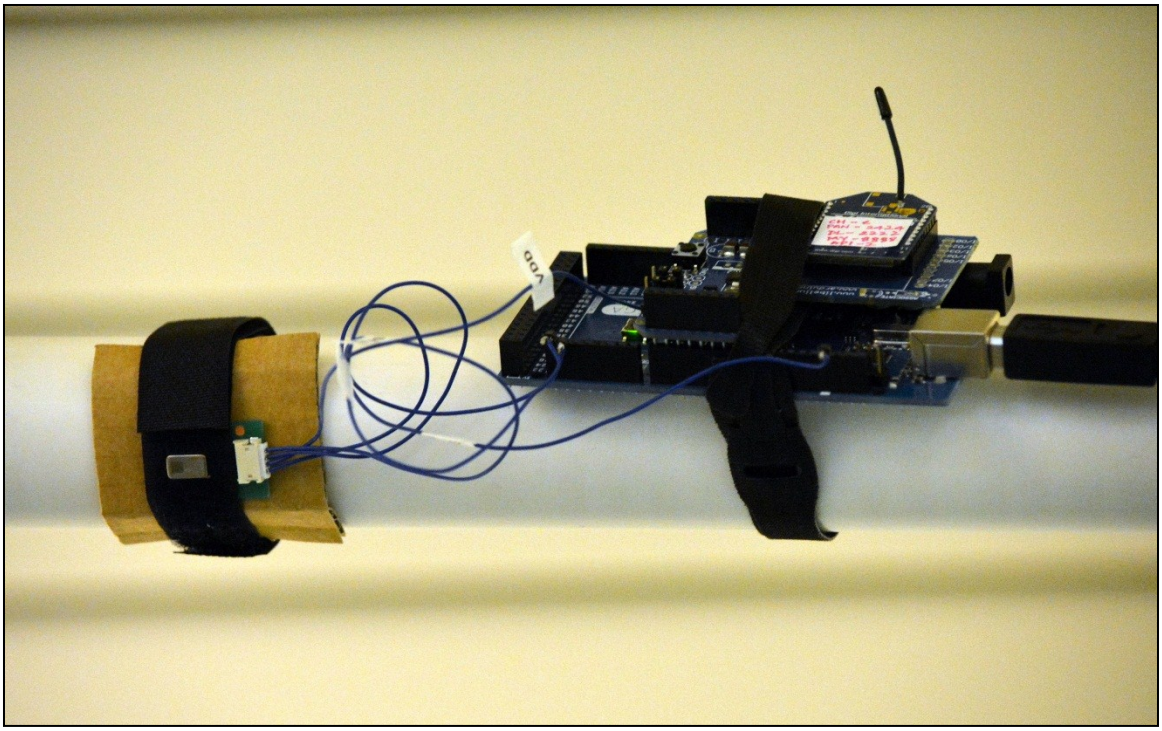

Figure 3.11 GridEye sensor node

GridEye sensor node is shown in Figure 3.9. The sensor node is mounted on a support and focused on the test bed.

.

3.3 Test Bed Setup

A Smart Home test bed was set up for the experiments. The dimensions of the test bed are 16x22ft. It simulates a small one bedroom apartment. It includes a living room, a bedroom, a kitchen and a bathroom. Figure 3.10 shows a top view (left picture) and 3D view (right picture) of the mock apartment designed on the test bed. Autodesk Homestyler application was used to generate this figure [34].

Figure 3.12 Top view and 3D view of mock apartment

The test bed also contains an indoor localization system. This system provides ground truth location values, which simulates an indoor GPS system. The system is manufactured by Natural Point Inc [35] which includes 12 V100:R2 cameras. These cameras are mounted around the test bed so that every part of the test bed is in focus by at least three cameras. In order to track a human subject, special reflective markers are placed over the head. These special reflective markers are tracked by the Optitrack system which provides the position of the human. Using the position data trajectories, the human path could be determined. Figure 3.11 shows the test bed with the Optitrack system, PIR sensors and GridEye sensors.

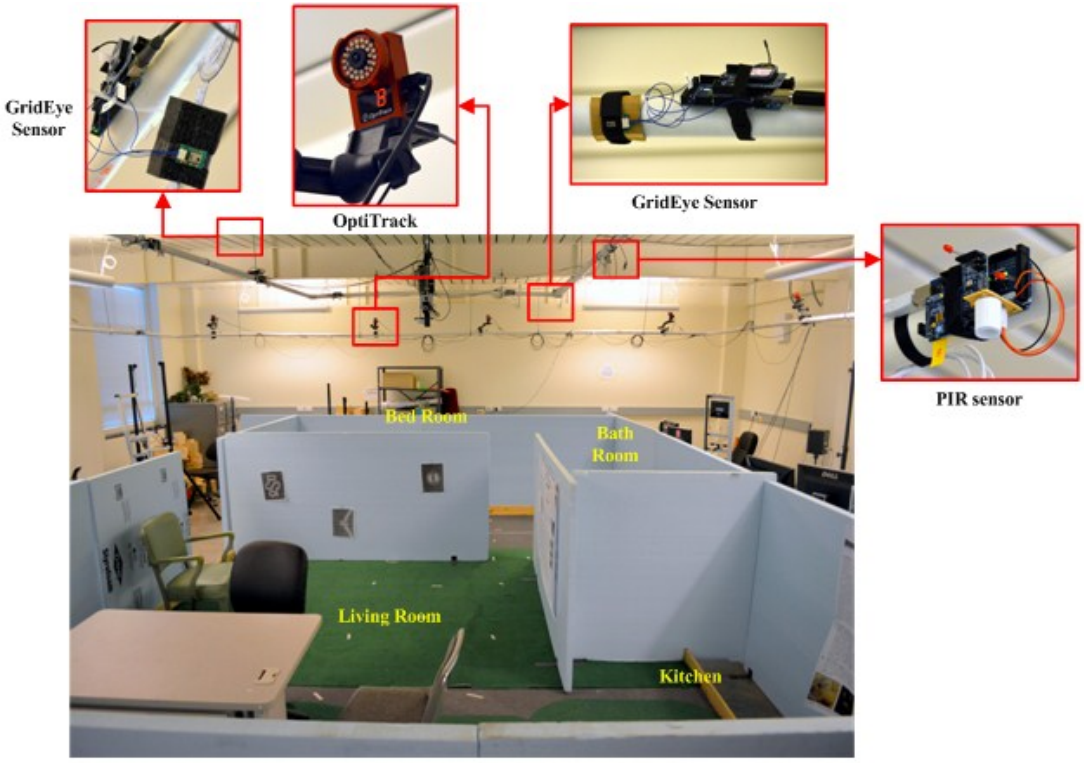

Figure 3.13 Test bed with OptiTrack system and Infrared Sensors

3.3.1 Sensor Placement

The PIR and GridEye sensors are strategically placed at various locations. The GridEye sensors are placed in the living room and the bedroom. The PIR sensors are placed in the kitchen and the bathroom. Since the GridEye sensor can localize and recognize the human activity as well, they were placed in the living room and bedroom. It was more appropriate to use the PIR motion sensor in bathroom and kitchen where just localization is sufficient. Moreover the temperature emissions from equipment in kitchen like stove, conventional oven, microwave oven interfere with activity detection by the GridEye sensor. Hence just a PIR sensor was used to localize the human in the kitchen. Figure 3.11 shows the sensor placement around the test bed.

CHAPTER VI

4. GRIDEYE SENSOR CALIBRATION

Calibration is an important step in transformation of pixel coordinates to real world coordinate system. In this chapter we explain calibration of GridEye sensor used in our thesis

The GridEye sensor is used to localize the human within its field of view. The human can be detected by the sensor as higher temperature object compared to the background. And using the localization algorithm, the human is localized in the pixel coordinates. But in order to transform the pixel coordinates to spatial coordinates, we have to calibrate the sensor. A camera is calibrated to remove distortion and to find the relation between the pixel units and real world units. Most of the traditional cameras are calibrated using the checkered board as the calibration target. Using calibrations one can estimate the intrinsic and/or extrinsic parameters. Intrinsic parameters are the internal characteristics of the camera such as focal length, skew and distortion. The extrinsic parameters are the position and orientation of the camera. In order to calibrate, a pattern such as the checkered board is printed and mounted on a flat surface. Many pictures of this calibration target are taken at different orientations and distances. Later using these pictures the calibration code is executed to find out the calibration results. The results are saved into a file [36][37]. All these procedures could be followed if the camera is a pin-hole camera, or a camera with high resolution.

The thermal array sensor that is used in this experiment is of very low resolution to carry out this procedure. Hence a manual calibration is required. Since we are using a thermal sensor, a heat source is used as the calibration target.

Initially in our experiments to calibrate the sensor, several heat sources were tried. A regular 90W Incandescent light bulb produced enough heat to be differentiated from the background, but with distance it diminished drastically to be identified. A candle produces a lot of heat but the size of the candle was too small to be detected at larger distance. Also using a candle was unsafe and dangerous in a lab environment. Work lamps with halogen bulbs were also used for calibration. The 500W halogen bulb produces 20,000 lumen output and very high temperature that could be detected at great distances by the Grid Eye sensor.

As the work lamps are turned ON the temperature of the lamp increases drastically. After 2-4 minutes the lamps are turned off and are brought in the field of view of the sensor. An application that displays the real-time temperature of each pixel of the sensor is executed on the computer. The lamp was placed in the center of the selected pixel in real space. The positions were marked and later the ground truth values were determined using the Optitrack system. Using the pixel values and the positions in real world a relation between them was determined. Nine pixel and real world pairs were collected. Using these values two equations were formed; one equation for the x-axis and other for y-axis lines. Using these equations one could estimate the real world coordinates using the pixel values. A polynomial of degree ‘n’ was created using the data pairs. The polynomial was determined in a least square sense. The coefficients of both the polynomials were saved. Later the real world coordinates was evaluated at the particular pixel value using these coefficients. But this method was not accurate enough when experiments were conducted. This was due to the fact that the heat source was placed on the ground during calibration. But the human subject produces heat at an elevated position from the ground. In order to compensate this, an offset was added to during the experiments. But after several experiment, this method

produced results that weren't good enough. It was difficult to formulate a relationship between the calibrated values and the human temperatures.

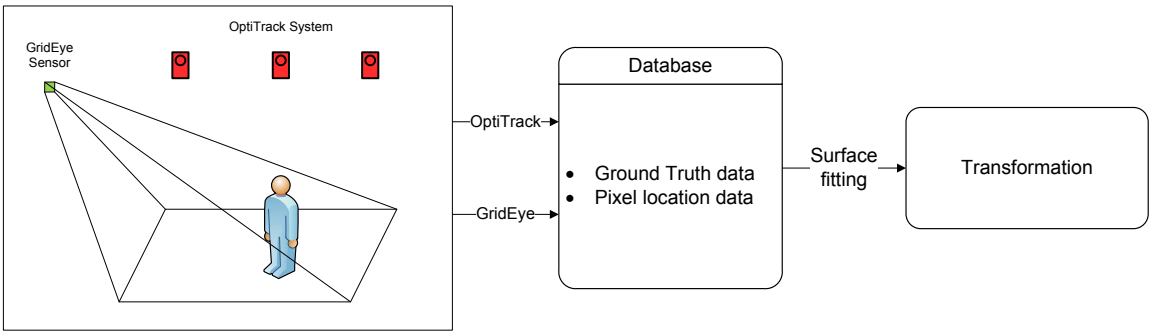

Figure 4.1 Flowchart of the GridEye sensor calibration

Later the human subject was considered as the heat source for calibration. Figure 4.1 shows flowchart of the GridEye sensor calibration. The human subject stood in the field of view of the sensor at different points as shown in Figure 4.1. The sensor data was recorded at each of these points. The ground truth values at each position the human subject stood was recorded using the OptiTrack system. The sensor data was processed and a temperature image above a certain threshold was calculated. The centroid of hot pixels above the threshold was calculated and saved. Now a relationship between the sensor pixel values and the ground truth values was calculated. Initially the x-axis pixel values and x-axis ground truth values were related with a polynomial equation and y-axis pixel values and y-axis ground truth values were related with another polynomial equation. Even though this method of calibration produced good results, the output was skewed. This was because the field of view of the sensor is skewed when placed at an angle. In order to eliminate this, ground truth x-axis values were related to both x and y axis pixel values and similarly the y-axis ground truth values were related to both x and y axis pixel values. This method of calibration produces two surface equations. These equations were later used to transform the x and y axis pixel values to real world coordinates.

CHAPTER VII

5. HUMAN LOCALIZATION

Human localization plays an important role in locating the human and analyzing his/her behavior. This chapter explains the algorithm used in our research in localizing the human. PIR sensors and the GridEye sensors are used in locating the human. The data obtained from these sensors are processed using our algorithm to get the location of the human in real world coordinates.

5.1 Overall Approach

In this thesis we used GridEye and the PIR sensor to localize the human. The GridEye sensor provides sufficient data to localize the human in its field of view. Normal body temperature ranges from 97.8 degrees F (or Fahrenheit, equivalent to 36.5 degrees C, or Celsius) to 99 degrees F (37.2 degrees C) for a healthy adult [38]. The average room temperature ranges from 20 to 23.5 °C (68.0 and 74.3 °F) with an average of 21 °C (70 °F) [39]. Clearly, there is difference in the temperature between the room and the normal human temperature. In order to easily identify the human's presence, we performed background subtraction. Initially when the system is activated, we assume that the room is unoccupied. During that time the GridEye captures the temperature data of the unoccupied room. Hence temperatures of all pixels were in and around the room temperature. Two to four seconds of unoccupied room was captured and mean of all frames in that time was calculated and saved. In order to detect a human, the real time frame was subtracted with the mean background frame.

This helped us to remove the stationary background and detect the foreground object. Since the object of interest was of higher temperature than the background temperature, the object of interest became more prominent after background subtraction. All the pixels of the background were close to zero after the background subtraction. There was normal distribution with the mean close to zero. And the values of objects of interest were outside that normal curve.

Before the background subtraction all the images were first interpolated. The sensor data has a low resolution of just 8x8 pixels, this is very discrete to produce a smooth trajectory for the path travelled by the human. Interpolation helps us to produce a smooth trajectory. In our experiments Bicubic interpolation method was used for interpolation and the images were scaled by a factor of 4. In this method, the output pixel value was a weighted average of pixels in the nearest 4-by-4 neighborhood.

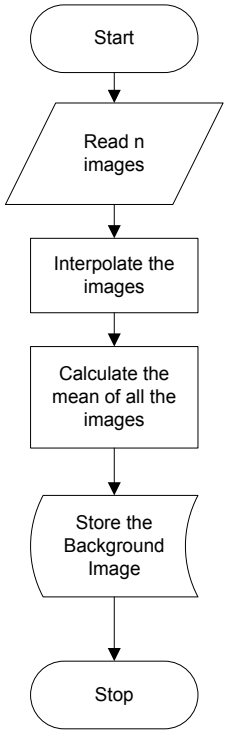

Figure 5.1 Flowchart for Background Subtraction

Initially, it is necessary that field of view of sensor was not occupied by human before the sensor was turned ON. The system recorded specified number of images for background subtraction. The images were interpolated and later the mean of all these images was calculated and saved as background image. This image was later used for background subtraction for determining the human location. Flowchart for background subtraction is shown in Figure 5.1.

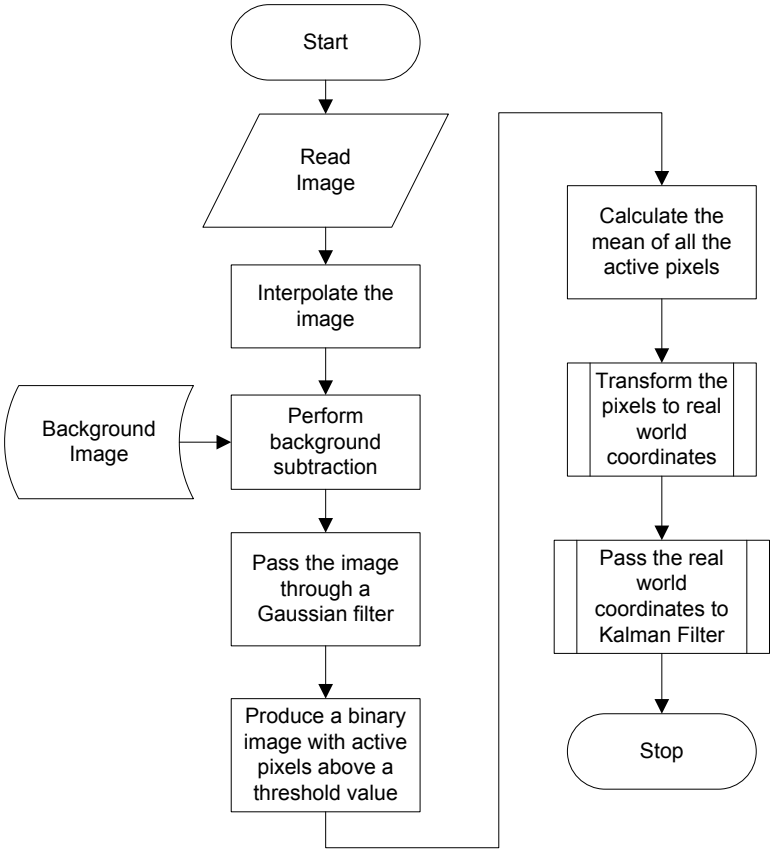

Figure 5.2 Flowchart of image processing of Raw Sensor data

After the background image is saved, the system starts reading the data to locate the human. Figure 5.2 explains the processing done on the raw data received from the GridEye sensor. The image was first interpolated. An original sensor image and interpolated image are shown in Figure 5.3. It can clearly be seen that the interpolated data is more continuous and easier to visualize the human's presence. The interpolated data was then subtracted by the background

image saved earlier. After background subtraction, the foreground human subject was clearly visible since the static background was removed. The image was then passed through a Gaussian filter. This helped us to remove any random noise in the image. Figure 5.4 shows the image after being passed through the Gaussian filter. After this a binary image called Threshold Image is created. This image contains active pixels only at positions with temperature values above a threshold value. The histogram in Figure 5.4 shows the pixel distribution. We can see that there is normal distribution about zero. This is usually the pixels of the background. These pixels can be ignored. The pixels of interest are of higher temperature. A specific threshold value is selected such that the foreground object is detected and yet all the other pixels belonging to the static background is removed. The figure shows the threshold image in 2D and 3D. In order to determine the location of the human, the centroid of the active pixels in the threshold binary image is calculated. The centroid gives the center of the heated object. This location in pixel coordinates was converted into real world coordinates by passing the pixels through the surface equations determined during the calibration process. The real world coordinates was then given as input to the Kalman filter to remove noise and get a smooth trajectory.

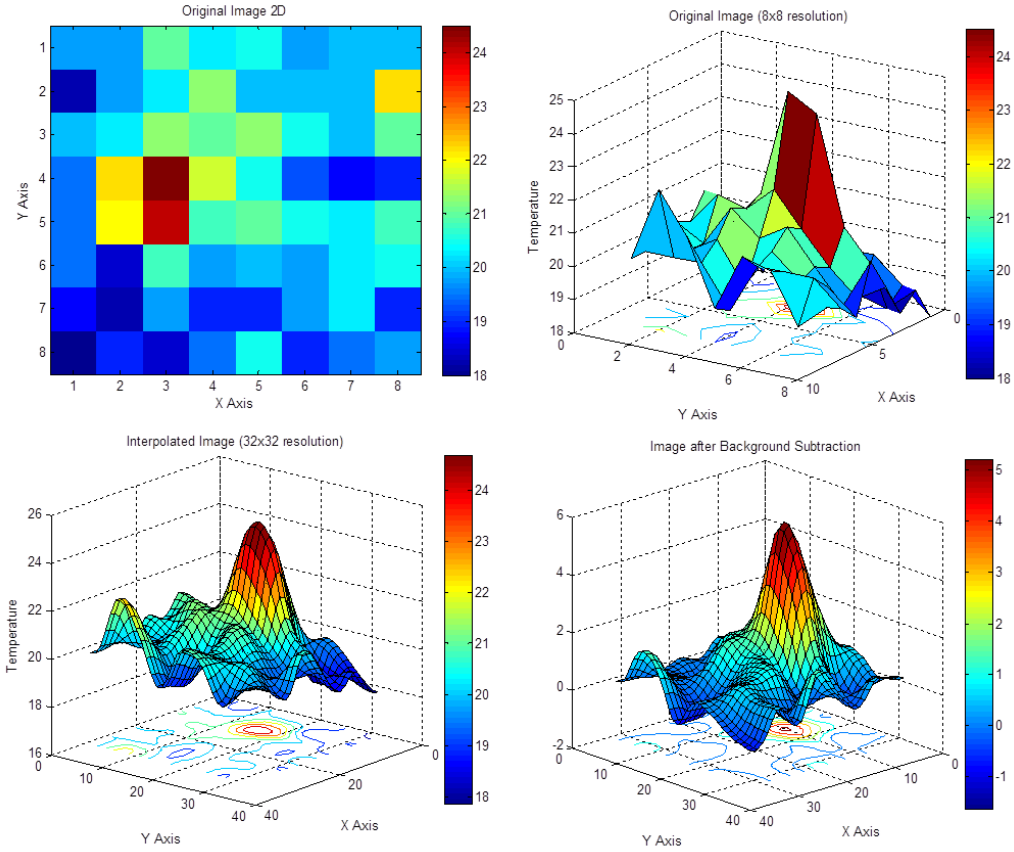

Figure 5.3 Original Image in 2D (Top Left), Original Image in 3D (Top Right), Interpolated Image (Bottom Left), Interpolated image after Background Subtraction (Bottom Right)

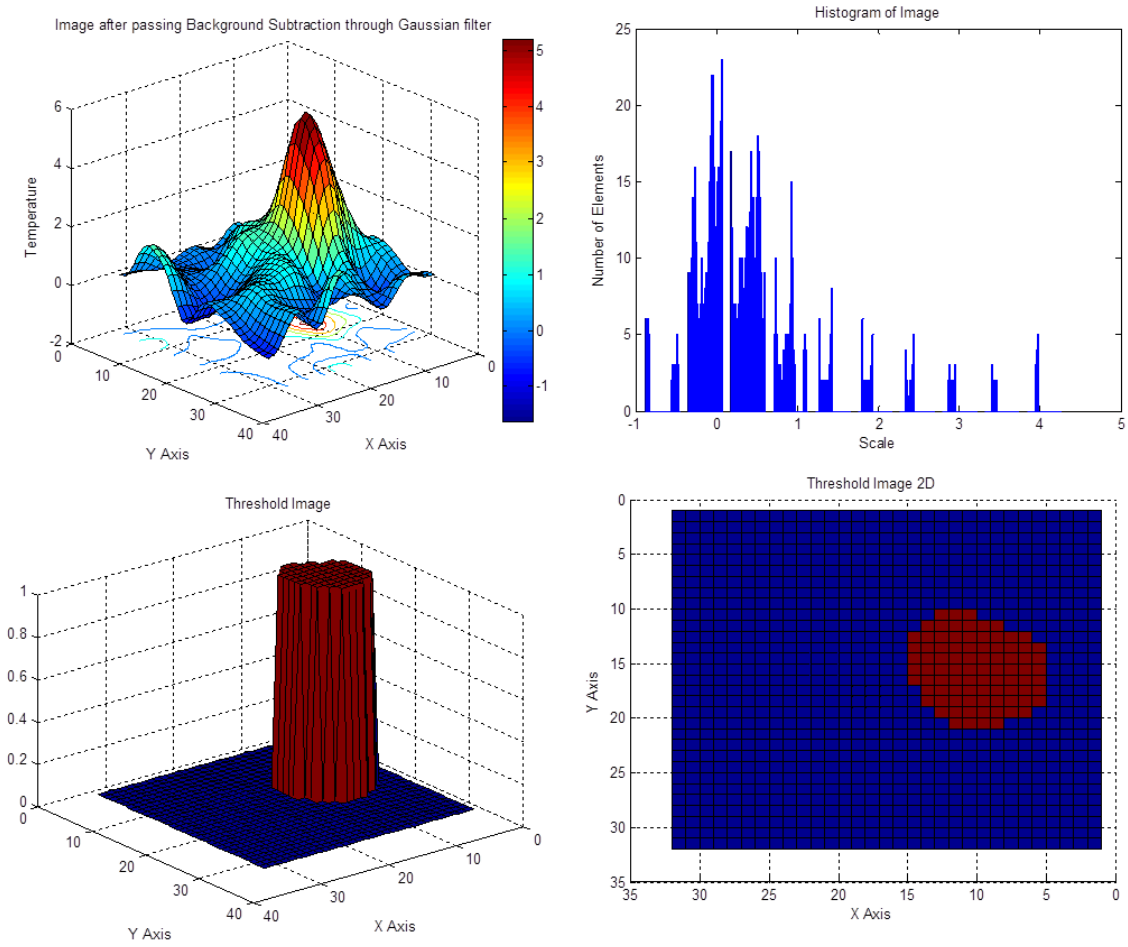

Figure 5.4 Image after passing through Gaussian filter (Top Left), Histogram of Gaussian Image (Top Right), Threshold Image in 3D (Bottom Left), Threshold Image in 2D (Bottom Right)

5.2 Kalman Filter

Kalman filter is an algorithm that is generally used to reduce noisy data and provide estimate of parameters of interest [40]. Kalman filter is used in many applications, including Global Positioning System receivers, tracking objects, phase-locked loops in radio equipment. They are also used in many computer vision applications. In our thesis work, we used Kalman filter to track the human subject and remove the noise in the system. We used the Kalman filter as suggested by Ramsey Faragher [40] and Dave [41].

In our experiments we are tracking a human subject who could travel in two dimensions in real world. The human subject can travel in both X and Y directions. Hence we assume a standard model of motion in equations below.

$$\boldsymbol{x_{t+1} = x_t + v_t T + \frac{1}{2} a T^2} \quad (5.1)$$

$$\boldsymbol{v_{t+1} = v_t + aT} \quad (5.2)$$

$$\boldsymbol{y_{t+1} = y_t + v_t T + \frac{1}{2} a T^2} \quad (5.3)$$

$$\boldsymbol{v_{t+1} = v_t + aT} \quad (5.4)$$

Where

- v_t is velocity and a is acceleration and T is time elapsed between time epochs t and $t-1$.

Equations 5.1 and 5.2 are in x direction and Equations 5.3 and 5.4 are in y direction. The Kalman filter assumes that the state of a system at time *t* evolved from the prior state at time *t-1* according to the Equation 5.5, which is the state update equation.

$$\overline{x}_t = Ax_{t-1} + Bu_t + w_t \quad (5.5)$$

Where

- $\overline{x}_t$ is the current state vector containing the position and velocity for the system at time *t*.
- *A* is the state transition matrix which applies the effect of each system state parameter at time *t-1* on the system parameter at time *t*.
- x_{t-1} is the prior state vector.

- B is the control input matrix which applies the effect of each control input parameter in the vector u_t on the state vector.
- u_t is the vector containing control input acceleration.
- w_t is the vector containing the process noise terms for each parameter in the state vector. The process noise is assumed to be normal distribution with mean zero and covariance given by covariance matrix Q_t.

The measurements of the system are given by the measurement update model Equation 5.6.

$$\overline{\boldsymbol{z}}_{\boldsymbol{t}} = \boldsymbol{C}\overline{\boldsymbol{x}}_{\boldsymbol{t}} + \boldsymbol{v}_{\boldsymbol{t}} \tag{5.6}$$

Where

- $\overline{z}_t$ is the vector of measurements
- C is the transformations matrix that maps the state vector parameters into the measurement domain.
- v_t is the vector containing the measurement noise terms for each observation in the measurement vector. The measurement noise is assumed to be zero mean Gaussian white noise with covariance R_t.

The state vector $\overline{x}_t$ contains the position and velocity of the human in two directions X and Y given by Equation 5.7.

$$\overline{\boldsymbol{x}}_{\boldsymbol{t}} = \begin{bmatrix} \boldsymbol{x}_{\boldsymbol{t}} \\ \boldsymbol{y}_{\boldsymbol{t}} \\ \dot{\boldsymbol{x}}_{\boldsymbol{t}} \\ \dot{\boldsymbol{y}}_{\boldsymbol{t}} \end{bmatrix} \tag{5.7}$$

From equation 5.1, 5.2, 5.3 and 5.4 we can derive the linear equations as Equation 7.8.

$$\begin{bmatrix} x_t \\ y_t \\ \dot{x}_t \\ \dot{y}_t \end{bmatrix} = \begin{bmatrix} 1 & 0 & T & 0 \\ 0 & 1 & 0 & T \\ 0 & 0 & 1 & 0 \\ 0 & 0 & 0 & 1 \end{bmatrix} \begin{bmatrix} x_{t-1} \\ y_{t-1} \\ \dot{x}_{t-1} \\ \dot{y}_{t-1} \end{bmatrix} + \begin{bmatrix} \frac{T^2}{2} \\ \frac{T^2}{2} \\ T \\ T \end{bmatrix} a \tag{5.8}$$

So when we compare Equation 5.8 this with Equation 5.5 we have

$$A = \begin{bmatrix} 1 & 0 & T & 0 \\ 0 & 1 & 0 & T \\ 0 & 0 & 1 & 0 \\ 0 & 0 & 0 & 1 \end{bmatrix} \text{ and } B = \begin{bmatrix} \frac{T^2}{2} \\ \frac{T^2}{2} \\ T \\ T \end{bmatrix} \tag{5.9}$$

In the measurement update model, we are measuring and recording only the position of the human, hence the transformation matrix C will be limited only to the x and y positions (Equation 5.10).

$$C = \begin{bmatrix} 1 & 0 & 0 & 0 \\ 0 & 1 & 0 & 0 \end{bmatrix} \tag{5.10}$$

The standard Kalman filter equations for the prediction stage are given by Equations 5.11 and 5.12

$$\overline{x}_{t|t-1} = A\overline{x}_{t-1|t-1} + Bu_t \tag{5.11}$$

$$P_{t|t-1} = AP_{t|t-1}A^T + Q_t \tag{5.12}$$

Where P_t is the covariance matrix, and Q_t is the process noise covariance matrix associated with noisy control inputs (Equation 5.13).

$$Q_t = \begin{bmatrix} \frac{T^4}{4} & 0 & \frac{T^3}{2} & 0 \\ 0 & \frac{T^4}{4} & 0 & \frac{T^3}{2} \\ \frac{T^3}{2} & 0 & T^2 & 0 \\ 0 & \frac{T^3}{2} & 0 & T^2 \end{bmatrix} \times \sigma_N^2 \tag{5.13}$$

Where, σ_N is process noise or variability in how fast the human is moving (standard deviation of acceleration).

The measurement update equations are given by Equations 5.14 and 5.15

$$\overline{\boldsymbol{x}}_{\boldsymbol{t|t}} = \overline{\boldsymbol{x}}_{\boldsymbol{t|t-1}} + \boldsymbol{K_t}(\boldsymbol{z_t} - \boldsymbol{C}\overline{\boldsymbol{x}}_{\boldsymbol{t|t-1}}) \tag{5.14}$$

$$\boldsymbol{P_{t|t}} = \boldsymbol{P_{t|t-1}} - \boldsymbol{K_t C P_{t|t-1}} \tag{5.15}$$

Where

$$\boldsymbol{K_t} = \boldsymbol{P_{t|t-1}C^T}(\boldsymbol{CP_{t|t-1}C^T} + \boldsymbol{R_t})^{-\mathbf{1}} \tag{5.16}$$

Where

$\overline{x}_{t|t}$ is the state vector following data fusion

$\overline{x}_{t|t-1}$ is the state vector before data fusion, i.e., the prediction

$P_{t|t}$ is covariance matrix (confidence) following data fusion

$P_{t|t-1}$is covariance matrix (confidence) before data fusion

z_t is the measurement vector

K_t is the Kalman gain

R_t is the uncertainty matrix associated with a noisy set of measurements

$$\boldsymbol{R_t} = \begin{bmatrix} \boldsymbol{\sigma_x^2} & \mathbf{0} \\ \mathbf{0} & \boldsymbol{\sigma_y^2} \end{bmatrix} \tag{5.17}$$

Where $\sigma_x^2$and σ_y^2 are variance in measurement in x and y directions respectively.

These equations were used in removing the noise in the system and predicting the position of the human.

5.3 Location Accuracy Evaluation

After using the Kalman filter, a trajectory of the path travelled by the human is obtained. In order to check the accuracy of trajectory of the system we used the OptiTrack system. It is an indoor localization system which can be treated like an indoor GPS. Special markers were placed on the human subject to be tracked by the OptiTrack system. The position provided by the OptiTrack system was saved which was later used to plot the trajectory. To determine the location accuracy of GridEye sensor, the trajectories of the human path produced by GridEye sensor and OptiTrack system were compared. Each point of trajectory formed by GridEye sensor was compared with trajectory formed by OptiTrack system. Point to point distance calculated was the Euclidean distance between the points. In order to calculate the error between the two trajectories, the distance between each point in the trajectory of GridEye to the nearest point in the trajectory formed by the OptiTrack was calculated. In Figure 5.5 assume line P is trajectory obtained from the GridEye sensor and line Q is the trajectory obtained from the OptiTrack system. The points q1, q2, q3 and q4 on line Q are closest to the points p1, p2, p3 and p4 on line P respectively. The Euclidean distance between these points was calculated to determine the accuracy.

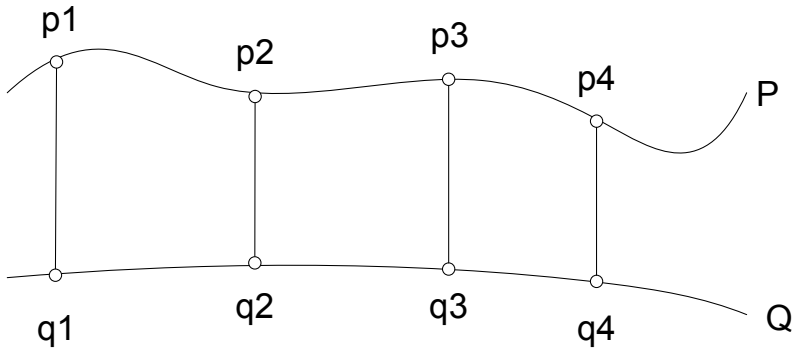

Figure 5.5 Distance between points on two lines.

The two dimensional Euclidean distance between two points is given by Equation 5.18.

$$\boldsymbol{d_{(p,q)}} = \sqrt{(\boldsymbol{p_1} - \boldsymbol{q_1})^2 + (\boldsymbol{p_2} - \boldsymbol{q_2})^2} \tag{5.18}$$

Where $p = (p_1, p_2)$ and $q = (q_1, q_2)$ are two points in Euclidean plane.

Later the Root-Mean-Square (RMS) level of these distances is calculated. The root-mean-square level of a vector X is given by Equation 5.19 [42].

$$\boldsymbol{X_{RMS}} = \sqrt{\frac{1}{N}\sum_{n=1}^{N}|\boldsymbol{X_n}|^2} \tag{5.19}$$

with the summation performed along the specified dimensions.

CHAPTER VIII

6. ACTIVITY RECOGNITION

Activity recognition plays an important role in assisting elderly, sick and disabled [36]. By recognizing the activities of elderly person, we can keep a track of their daily routine. In this chapter we explain the algorithm used in our experiments for activity recognition. In our experiments we recognize several basic activities such as sitting on dining chairs, sitting on couch, sleeping, walking and standing. We use the supervised learning SVM algorithm for activity recognition of sitting on dining chairs, sitting on couch and sleeping.

6.1 Support Vector Machine

SVM is a supervised learning model that is used for classification and regression analysis. SVM is highly used in pattern recognition and data classification [43]. SVM was proposed by Vladimir N. Vapnik and Corinna Cortes in 1995 [44]. SVM initially generates a model based on the training data given to it. Later the new data is classified based on the model generated earlier. SVM classifies the data by finding a hyper-plane that separates all the data points belonging to two classes. The hyper-plane selected is such that the margin between the two classes is the largest.

Consider a data set x_i belonging to one of the two classes $y_i = -1\ or\ +1$ as shown in Figure 6.1. Here we assume that data set is linearly separable by drawing a line on a graph.

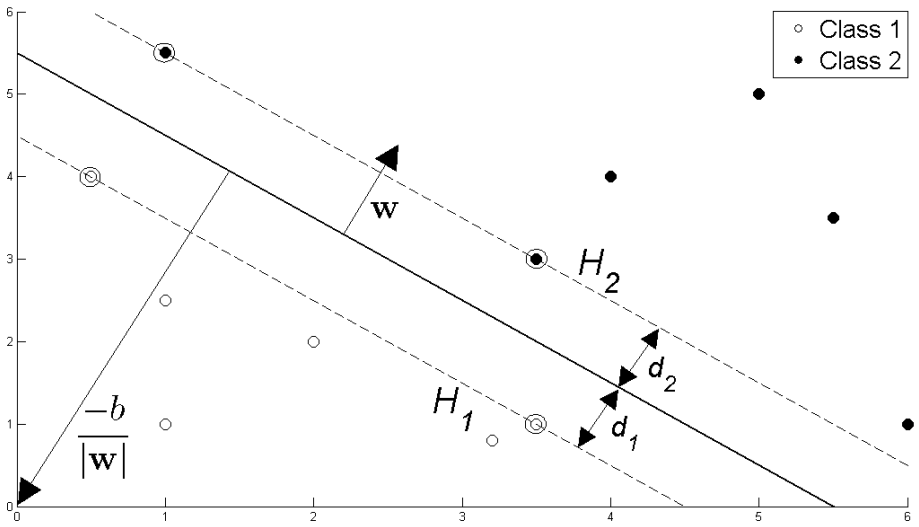

Figure 6.1 Hyperplane through two linearly separable classes [45]

In Figure 6.1 the hyperplane can be described by $w.x + b = 0$ where:

- w is normal to the hyperplane
- $\frac{b}{\|w\|}$is the perpendicular distance from the hyperplane to the origin.

The variables w and b are selected such that data can be classified as

$$\boldsymbol{x_i.w + b \geq +1} \text{ for } \boldsymbol{y_i = +1} \tag{6.1}$$

$$\boldsymbol{x_i.w + b \leq +1} \text{ for } \boldsymbol{y_i = -1} \tag{6.2}$$

The two planes H_1 and H_2 can be described as

$$\boldsymbol{x_i.w + b = +1} \text{ for } \boldsymbol{H_1} \tag{6.3}$$

$$\boldsymbol{x_i.w + b = -1} \text{ for } \boldsymbol{H_2} \tag{6.4}$$

The hyperplane's distance from H_1 is d_1 and distance from H_2 isd_2. The distances $d_1$and $d_2$are equal and that distance is known as SVM's margin. We have to maximize the margin such that

$$\boldsymbol{min}\frac{\mathbf{1}}{\mathbf{2}}\|\boldsymbol{w}\|^{\mathbf{2}} \text{ such that } \boldsymbol{y_i}(\boldsymbol{x_i}.\boldsymbol{w}+\boldsymbol{b})-\mathbf{1}\ \geq \mathbf{0}\quad \forall_{\boldsymbol{i}} \tag{6.5}$$

This optimization problem is solved using Lagrange multipliers. The formula is as below

$$\boldsymbol{L_P} = \frac{\mathbf{1}}{\mathbf{2}}\|\boldsymbol{w}\|^{\mathbf{2}} - \sum_{\boldsymbol{i}=\mathbf{1}}^{\boldsymbol{L}}\boldsymbol{\alpha_i}\boldsymbol{y_y}(\boldsymbol{x_i}.\boldsymbol{w}+\boldsymbol{b}) + \sum_{\boldsymbol{i}=\mathbf{1}}^{\boldsymbol{L}}\boldsymbol{\alpha_i} \tag{6.6}$$

where α are Lagrange multipliers.

The example explained is of two classes SVM that could be linearly separated. But in many cases nonlinear kernel functions are used to classify data in higher dimension. RBF (Radial Basis Function) or Gaussian is one of the most popular kernel functions. The formula for RBF is given in equation 6.7.

$$\boldsymbol{G}(\boldsymbol{x_1},\boldsymbol{x_2}) = \boldsymbol{exp}\left(\frac{\|x_1-x_2\|^2}{\mathbf{2}\boldsymbol{\sigma}^{\mathbf{2}}}\right) \tag{6.7}$$

In our thesis we used one class SVM to identify the specific activity. We used the RBF kernel function to map our data into higher dimensions. In one class SVM a boundary was formed with support vectors around the training data. Later when new data is given to the system, the system checks whether the new data falls within the boundary or outside.

There are two main parameters that control the characteristics of the boundary. A variable gamma controls the shape of the boundary. Higher value of gamma creates more support vectors and forms a boundary closely around the data points. The variable ν sets upper bound on the fraction of outliers (training examples regarded out-of-class) and, it is a lower bound on the number of training examples used as Support Vector [46][47]. A small value of ν leads to fewer support vectors, and, hence a smooth, crude decision boundary. A large value of ν leads to more

support vectors, and therefore, a curvy, flexible decision boundary. The optimal value of ν should be large enough to capture the data complexity and small enough to avoid overtraining [48].

Initially during training phase, the training data was used to train SVM model. Later during testing phase, the testing data was classified according to the SVM model created earlier. When the testing data was classified, the SVM score was observed. The score gives the likelihood that an observation comes from that class. A value of -1 and 0 indicate that the observation does not belong to the class. A value of 1 indicates that the observation belongs to the trained class.

In [25] Ryotaro Okada et al., provided raw data from the GridEye sensor to SVM as predictor data. This meant that the SVM had to operate on 64 dimensions for classification. In our experiments we provided processed data from the GridEye sensor as input to SVM. We provide five parameters as input as shown in Figure 6.2. The first two are the centroid of threshold image we created during localization process. This included the centroid location along x and y axis. The third parameter is area or number of active pixels in the threshold image. The fourth and fifth parameter are the mean and standard deviation of the temperature values of all the pixels in interpolated image that are active in the threshold image. Since we provided five data input, each of our observation was a point in 5 dimensional space. SVM was used to recognize the activity, hence the system was trained with correct activity data along with an appropriate label. The SVM produced a boundary around the training data. If the testing data was inside this boundary, then it was classified as the correct activity.

Centroid X-Coordinate	Centroid Y-Coordinate	Number of Active Pixel in Threshold Image	Mean temperature value of active pixels in interpolated image	Standard Deviation of temperature values of active pixels in interpolated image

Figure 6.2 SVM vector input

Walking and standing activities were recognized using location data of human. Walking and standing were recognized using speed at which human travelled inside apartment. If human remains stationary and the motion was less than a threshold, the human is assumed to be stationary. If human was travelling at a speed above a threshold value, then the human was assumed to be walking.

CHAPTER IX

7. EXPERIMENTS AND RESULTS

In this chapter we discuss several experiments conducted to localize and recognize the activity of the human. We have used a test bed which simulates a mock apartment to conduct our experiments. Results obtained from these experiments are provided in this chapter.

7.1 Data Acquisition

We used the test bed as a small one bedroom apartment. An elderly person was simulated to stay in this mock apartment. Data was collected from GridEye and PIR sensors. These sensors were connected to Arduino with Xbee shield and Xbee modules. Two Xbee sink nodes were connected to the computer to record the data. One Xbee sink node for each type of sensor. Two GridEye sensors were used in this project. One GridEye sensor was placed such that its field of view covers living room. Another GridEye sensor was placed in the bed room. Also, one PIR sensor was placed in kitchen and another in bathroom. These sensors were placed at a standard ceiling height of 8 feet. Figure 7.1 shows the sensor placements around the test bed.

Data from GridEye sensors was recorded at 10 frames per second. The PIR sensors transmitted wherever there was change of state. They transmitted data when motion was detected or when motion was stopped. To compare the accuracy of the system we used the OptiTrack system, which provides location data at a rate of 100 frames per second.

A human subject was asked to move around the mock apartment during the testing of the localization system. The human was asked to wear a cap with reflective markers on it to be detected by the OptiTrack system. GridEye sensor and PIR sensor detected the human due to heat produced by the human body.

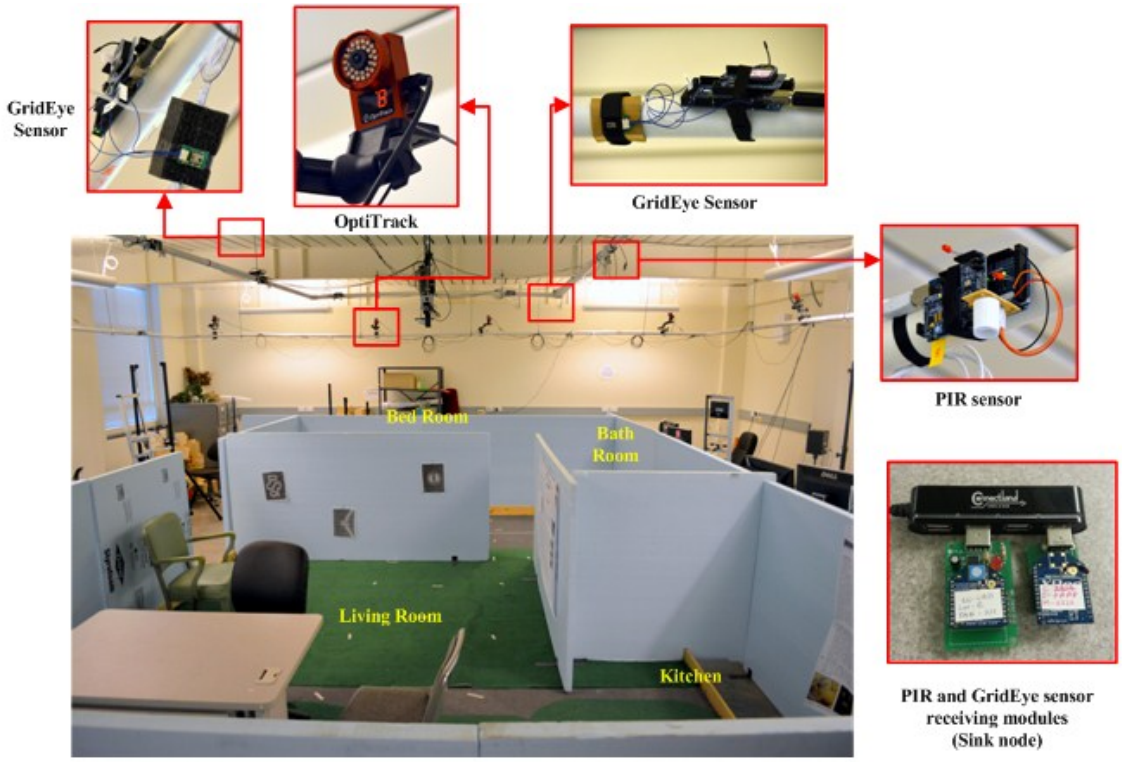

Figure 7.1 Test bed with PIR nodes, GridEye nodes and OptiTrack System and Sink node

7.2 Background Subtraction and Threshold selection

Background subtraction was performed on the GridEye sensor data to remove the static background and to highlight the foreground object of interest. After background subtraction, the image was passed through Gaussian filter to remove any random noise. A binary image was created with active pixels at places above a threshold value. To calculate the threshold value several experiments were conducted. Three minutes duration of frames were collected with the human subject walking around the field of view of the sensor and also without the human subject.

A histogram was plotted to check the density of pixels. The histogram of 1800 frames is shown in the Figure 7.2.

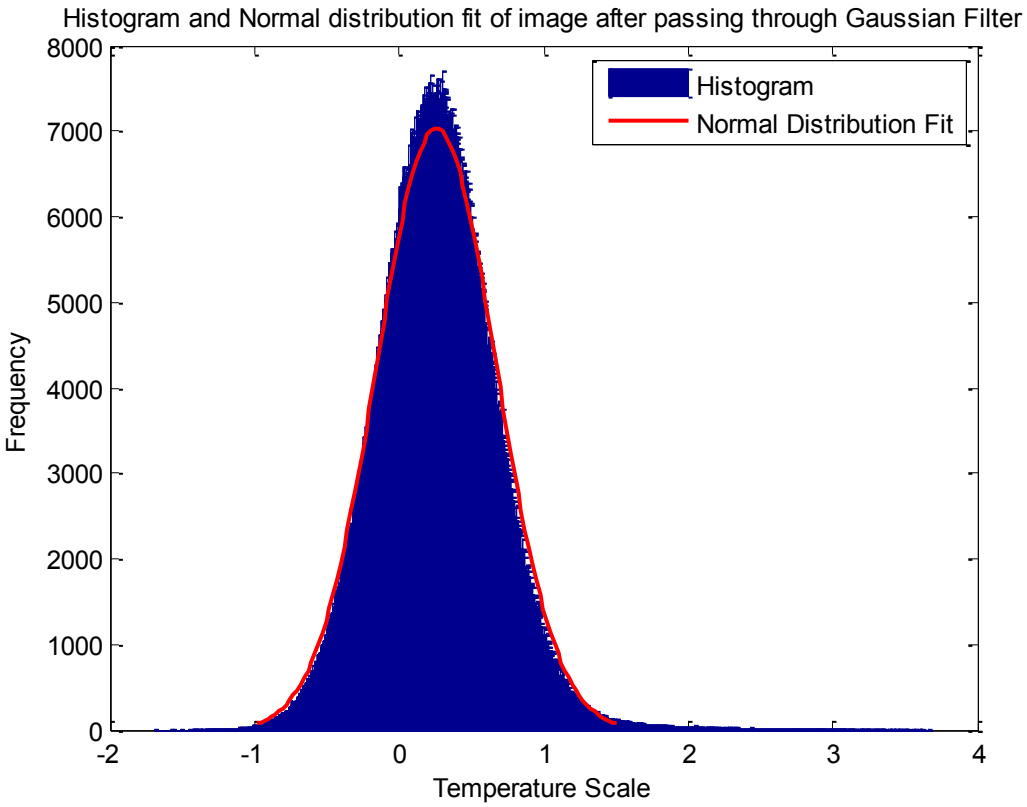

Figure 7.2 Histogram plot of pixels after passing through Gaussian filter

Most of the distribution pixels are static background. Pixels containing information about the human were present to the far right of the distribution. The mean and standard deviation was calculated and is shown in Table 7.1.

μ = 0.2586		**σ = 0.4136**
Normal Random Variable (x)		**Cumulative Probability P(X < x)**
μ + σ	0.6722	0.8412
μ + 2σ	1.0858	0.9772
μ + 3σ	1.4994	0.9987

Table 7.1 Normal Distribution calculation for threshold value

It can be seen from Table 7.1, that a threshold value of 1.5 removes 99.87% of the static background. Threshold value of 1.4 and 1.6 was also tested. With threshold value set to 1.4, the random noise was picked up and false positives were produced. With threshold value set to 1.6, we failed to detect the human in the far corners of field of view of the sensor. Hence a threshold value of 1.5 was used throughout our testing.

7.3 Calibration

Calibration of GridEye sensor was a crucial part of our experiments. Calibration provides us the transformation from pixel coordinates to real world coordinate. Initially the calibration was performed using the work lights as heat source as explained in Chapter 4. Later the human subject himself was used for calibration. The human subject stood in various locations in the field of view of the sensor and centroid of active pixels in the binary threshold image was calculated. The real world coordinates of the position where the human stood was determined using the OptiTrack system. One to one mapping of X and Y coordinates in pixel and real world was not accurate. The transformed coordinates were skewed due to the fact that the GridEye sensor was placed at an angle to the ground. Later surface fit was calculated to map the two coordinates systems. The linear surface fit plot for X coordinates and Y coordinates in real world system is given in Figure 7.2 and Figure 7.3.

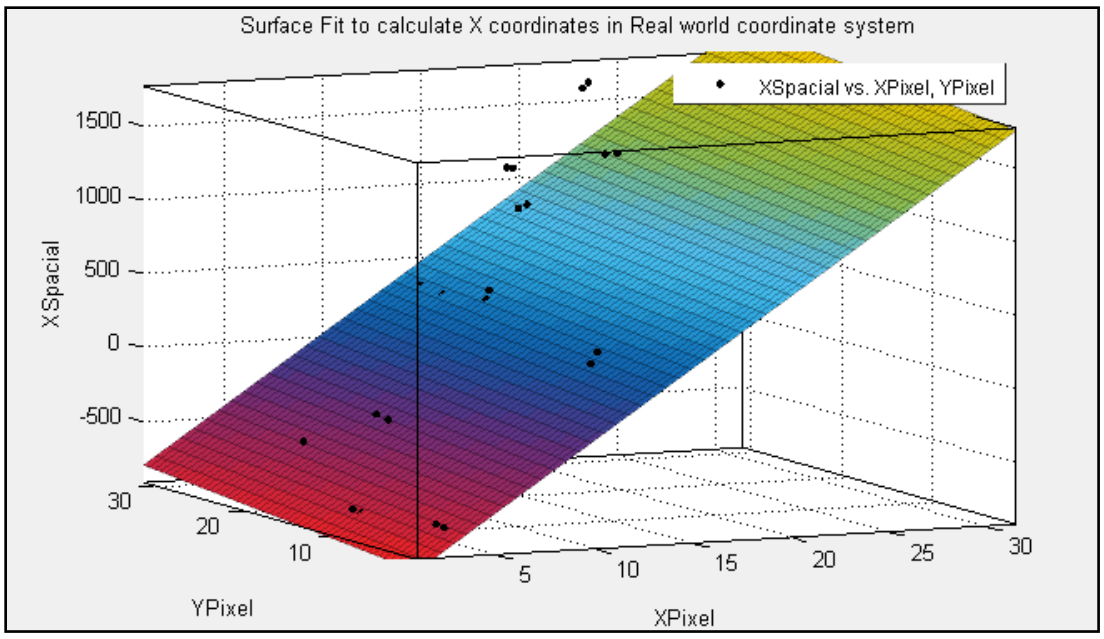

Figure 7.3 Surface fit for X coordinates in real world coordinate system

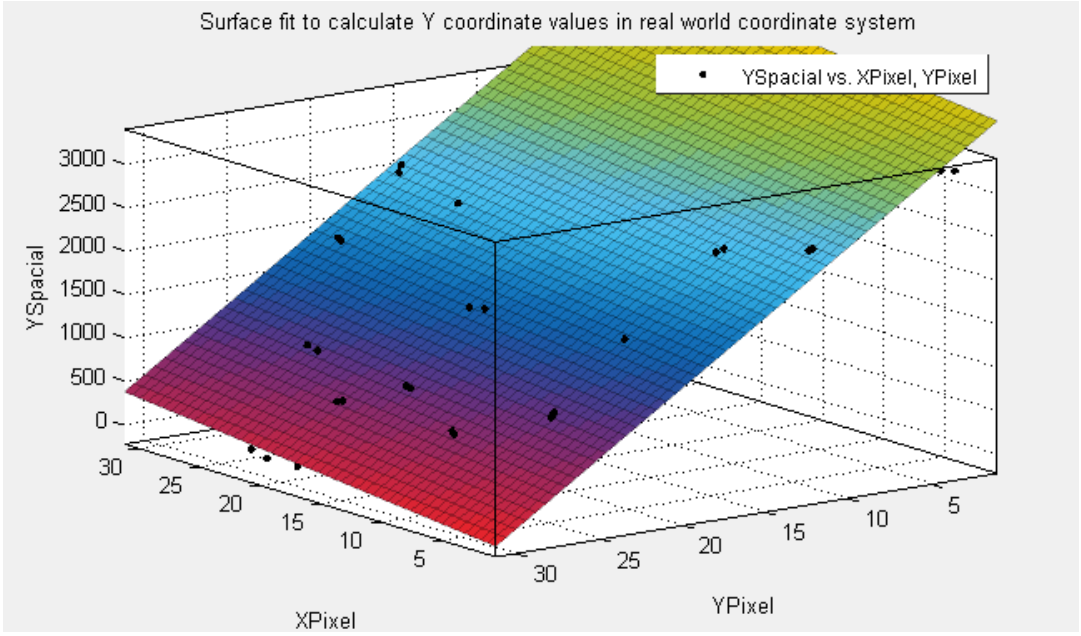

Figure 7.4 Surface fit for Y coordinates in real world coordinate system

To calculate the right type of surface fit that was most suitable for the transformation, several experiments were conducted. Similar to the calibration the human stood in the field of view of the sensor at 20 different positions. The real world coordinates was determined using OptiTrack

system. The centroid of the threshold image was calculated and fed to the transformation equations to find out the transformed real world coordinates. The Euclidean distance between the transformed values and the OptiTrack values was compared. Table 7.2 shows the error in transformation for different degrees in x & y of polynomial surface plot.

Surface fit for X coordinate		**Surface fit for Y coordinate**		**Error (in mm)**		
Degree in x	**Degree in y**	**Degree in x**	**Degree in y**	**Average**	**Max**	**Min**
1	1	1	1	382.9214	92.83739	415.65
1	2	1	1	352.946	87.74366	386.3367
2	1	1	1	346.0755	84.7957	383.1877
2	2	1	1	345.8127	81.31632	382.8228
1	1	1	2	245.3957	92.81563	269.97
1	2	1	2	204.8934	40.6528	222.2048
2	1	1	2	195.4909	62.36435	216.6835
2	2	1	2	194.8841	58.67658	216.0375
1	1	2	1	382.3458	91.57943	414.9881
1	2	2	1	352.6305	91.08821	385.6246
2	1	2	1	345.5437	83.41656	382.4697
2	2	2	1	345.2517	79.87712	382.1041
1	1	2	2	242.1444	93.53596	265.7649
1	2	2	2	200.1867	96.0479	217.0763
2	1	2	2	188.8998	37.71708	211.4211
2	2	2	2	187.4593	17.91188	210.759

Table 7.2 Error in distance for different degrees in x and y of polynomial surface plot

We can observe from Table 7.2 that degree 2 in x and y for both the surface fits has the least average, minimum and maximum error distance. Hence degree 2 in x and y for both the surface plots was selected in all our experiments for transforming the pixel coordinates to real world coordinates. The transformation equations used to convert the pixel coordinates to real world coordinates is shown in Equation 7.1 and 7.2.

$$\boldsymbol{surfacex(x,y) = p_{00} + p_{10} * x + p_{01} * y + p_{20} * x^2 + p_{11} * x * y + p_{02} * y^2} \quad \textbf{(7.1)}$$

Where,

$p_{00} = -808.4, p_{10} = 93.6, p_{01} = -15.86, p_{20} = -1.157, p_{11} = 2.036, p_{02} = -0.3041$

$$\boldsymbol{surfacey(x,y) = p_{00} + p_{10} * x + p_{01} * y + p_{20} * x^2 + p_{11} * x * y + p_{02} * y^2} \quad \textbf{(7.2)}$$

Where,

$p_{00} = 2844,\ p_{10} = 43.4,\ p_{01} = 48.07,\ p_{20} = -1.343,\ p_{11} = 0.579,\ p_{02} = -5.499$

The localization accuracy of each GridEye sensor was calculated. Later the accuracy of GridEye sensor along with PIR sensor was also calculated. Experiment results are explained the section below.

7.4 GridEye Sensor 1 Testing

GridEye sensor placed in the living room was named as GridEye sensor 1. The GridEye sensor 1 sensed an area close to 140 square feet. The measurement obtained with this sensor was compared with the data obtained from OptiTrack system. Figure 7.4 shows plot of path travelled by human as measured by GridEye sensor 1 and OptiTrack system.

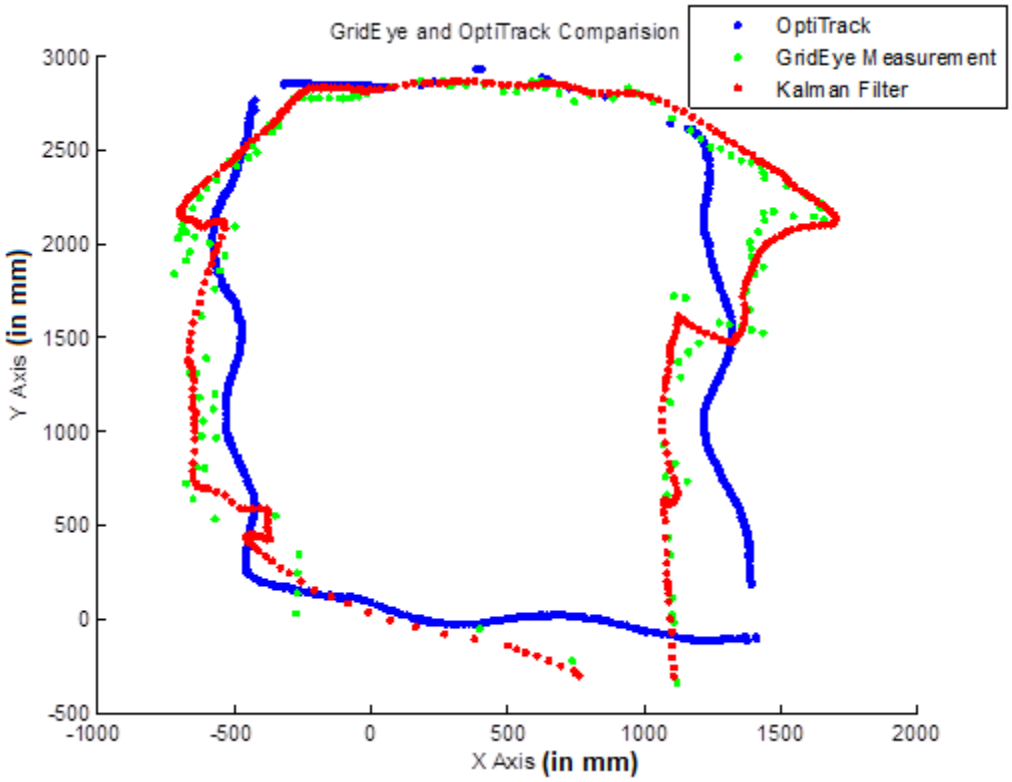

Figure 7.5 Plot of path travelled by human as calculated by GridEye sensor 1 and OptiTrack system

Error in measurement calculated using GridEye sensor 1				
Samples	**Average Error (in mm)**	**RMS Error (in mm)**	**Maximum Error (in mm)**	**Minimum Error (in mm)**
10	144.11	187.17	453.53	1.30

Table 7.3 Error in measurements by GridEye sensor 1

Error in measurements for 10 experiments conducted for GridEye sensor 1 is shown in Table 9.3. Error shown in Table 7.3 is the average, RMS, maximum and minimum Euclidean distance from each point in the measurements by GridEye sensor 1 with nearest OptiTrack measurements.

7.5 GridEye Sensor 2 testing

GridEye sensor 2 was placed in the bedroom of the mock apartment. GridEye sensor 2 sensed an area close to 80 square feet. Measurements obtained from this sensor were compared with data obtained from OptiTrack system. Figure 7.5 shows plot of path travelled by human as measured by GridEye sensor 1 and OptiTrack system.

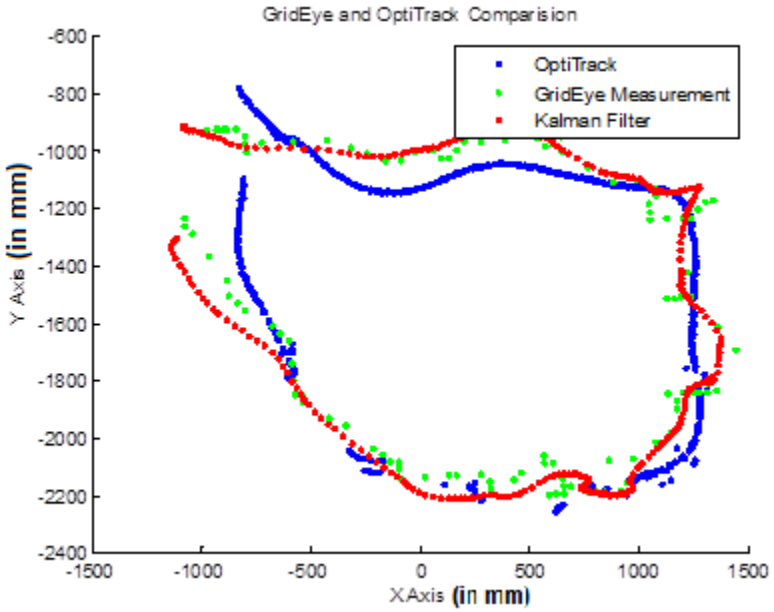

Figure 7.6 Plot of path travelled by human as calculated by GridEye sensor 2 and OptiTrack system

Error in measurement calculated using GridEye sensor 2				
Samples	**Average Error (in mm)**	**RMS Error (in mm)**	**Maximum Error (in mm)**	**Minimum Error (in mm)**
10	144.11	121.00	376.58	151.73

Table 7.4 Error in measurements by GridEye sensor 2

Table 7.4 shows error in measurements for 10 experiments conducted for GridEye sensor 2. Error shown in Table 7.4 is the average, RMS, maximum and minimum Euclidean distance from each point measured by GridEye sensor 1 with nearest OptiTrack measurements.

7.6 GridEye sensor 1 and sensor 2 testing

Later data from both GridEye sensor 1 and 2 were combined. Both sensors do not overlap with each other. Also since we assume that only one human lives in the apartment, presence of human in the field of view of these two sensors is mutual exclusive. Human was assumed to be present in the field of view of sensor which had the biggest active pixel area in the binary threshold image. Together the two sensors sensed an area close to 215 square feet. Measurements obtained from both sensors were compared with data obtained from the OptiTrack system. Figure 7.6 shows the plot of a path travelled by human as measured by GridEye sensor 1 and sensor 2 and OptiTrack system.

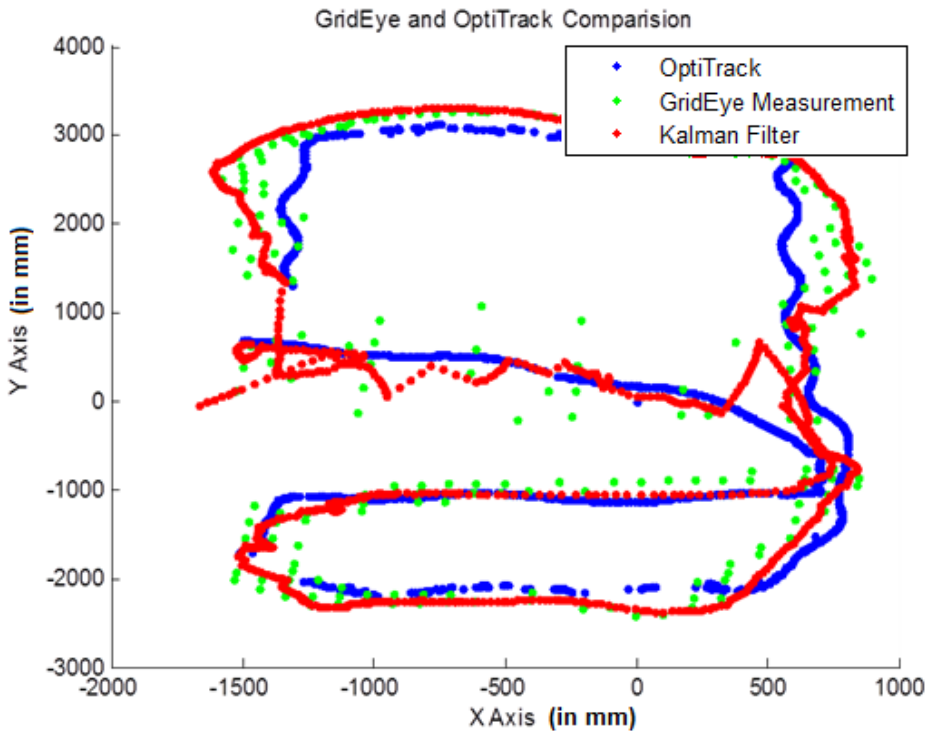

Figure 7.7 Plot of the path travelled by human as calculated by GridEye sensor 1 and sensor 2 and OptiTrack system

Error in measurement calculated using GridEye sensor 2				
Samples	**Average Error (in mm)**	**RMS Error (in mm)**	**Maximum Error (in mm)**	**Minimum Error (in mm)**
10	125.50	162.91	580.19	1.17

Table 7.5 Error in measurements by GridEye sensor 1 and sensor 2

Table 7.5 shows the error in measurements for 10 experiments conducted for GridEye sensor 1 and sensor 2. Error shown in Table 7.5 is the average, RMS, maximum and minimum Euclidean distance from each point measured by GridEye sensor 1 with nearest OptiTrack measurements.

7.7 GridEye sensor 1 and sensor 2 with PIR sensor testing

We tested combination of GridEye sensor 1 and sensor 2 with PIR sensor for localization. Combination of these sensors provided us localization of human throughout the mock apartment. When the PIR sensors were activated, human was assumed to be present in the room where the PIR sensor was mounted. The PIR sensors provided room level occupancy accuracy. The center of the PIR sensor was calculated and when the PIR sensor was activated, human was assumed to be present at center of PIR sensor. Accuracy of all these sensors combined was calculated similar the method used earlier. Figure 7.7 shows the plot of a path travelled by human as calculated by GridEye and PIR sensors and measured by OptiTrack.

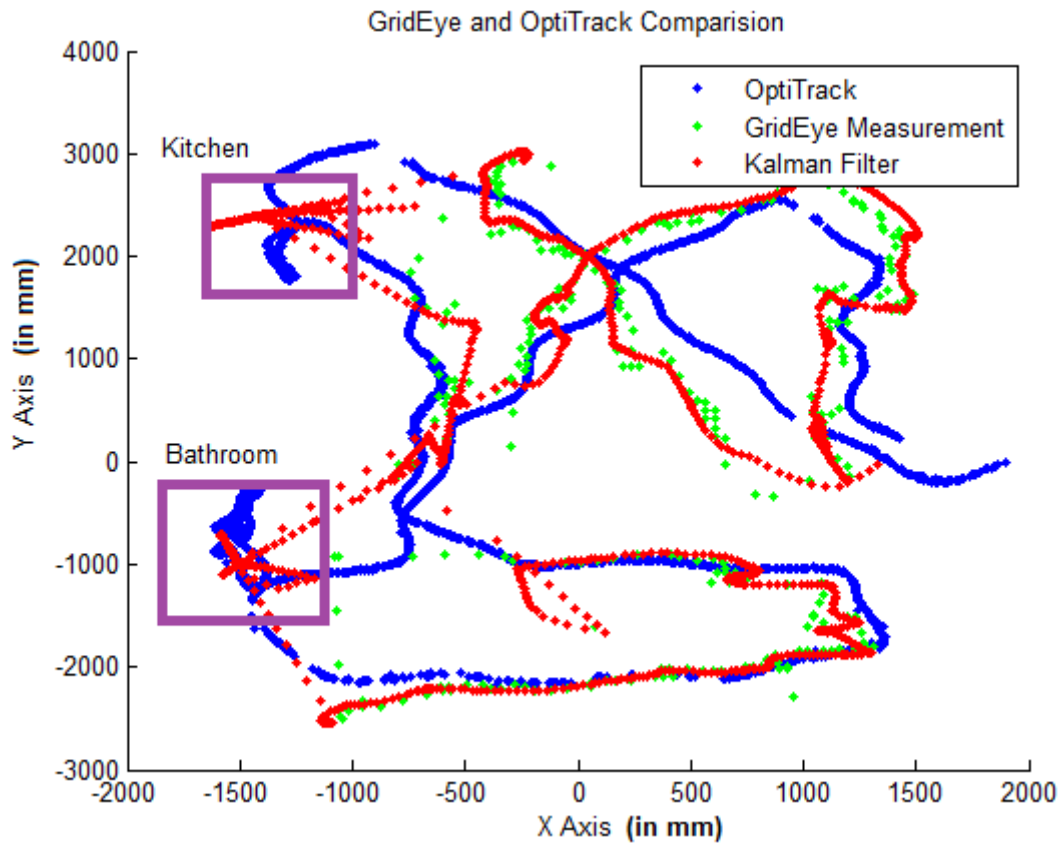

Figure 7.8 Plot of path travelled by human as calculated by GridEye and PIR sensor and OptiTrack system

Several experiments were conducted with the combination of these two sensors. Error in measurement calculated for 10 such experiments is tabulated in Table 7.6.

Error in measurement calculated using GridEye sensor 1,2 and PIR sensor				
Samples	**Average Error (in mm)**	**RMS Error (in mm)**	**Maximum Error (in mm)**	**Minimum Error (in mm)**
10	116.54	165.10	664.11	0.79

Table 7.6 Error in measurements by GridEye sensor 1 and sensor 2 and PIR sensors

From all experiments conducted we could estimate the position of human with an average accuracy of 116.54 mm.

7.8 Activity Recognition

In our research we used GridEye sensor to recognize four human activities. The four activities are sitting, standing, walking and sleeping. The human is assumed to sit at three locations such as chair 1, chair 2 and couch and sleep on bed. We assume that the furniture (Couch, chair 1, chair 2 and bed) are in fixed positions. Figure 7.8 shows the positions of furniture in the mock apartment. Standing and walking is recognized in the living room and the bed room. Recognition of these activities helps us to understand the daily routine of the person.

Sitting and sleeping activity recognition was done using the one-class SVM model. We provided processed data from the GridEye sensor as input to SVM. We provide five parameters as input. The five parameters are the centroid (x and y coordinates), active pixel area in the threshold image, mean and standard deviation of the temperature values of all the pixels in interpolated image that are active in the threshold image. Since we are using one-class SVM, we trained the model using correct predictor data. Human was asked to perform these activities and these actions were recorded using the GridEye sensor. The five predictor parameters mentioned above were calculated for all frames recorded. After training the model testing data was classified using the trained SVM model. The model was tested for error in recognizing the activity. The accuracy of the model was calculated by testing for false negative and false positive.

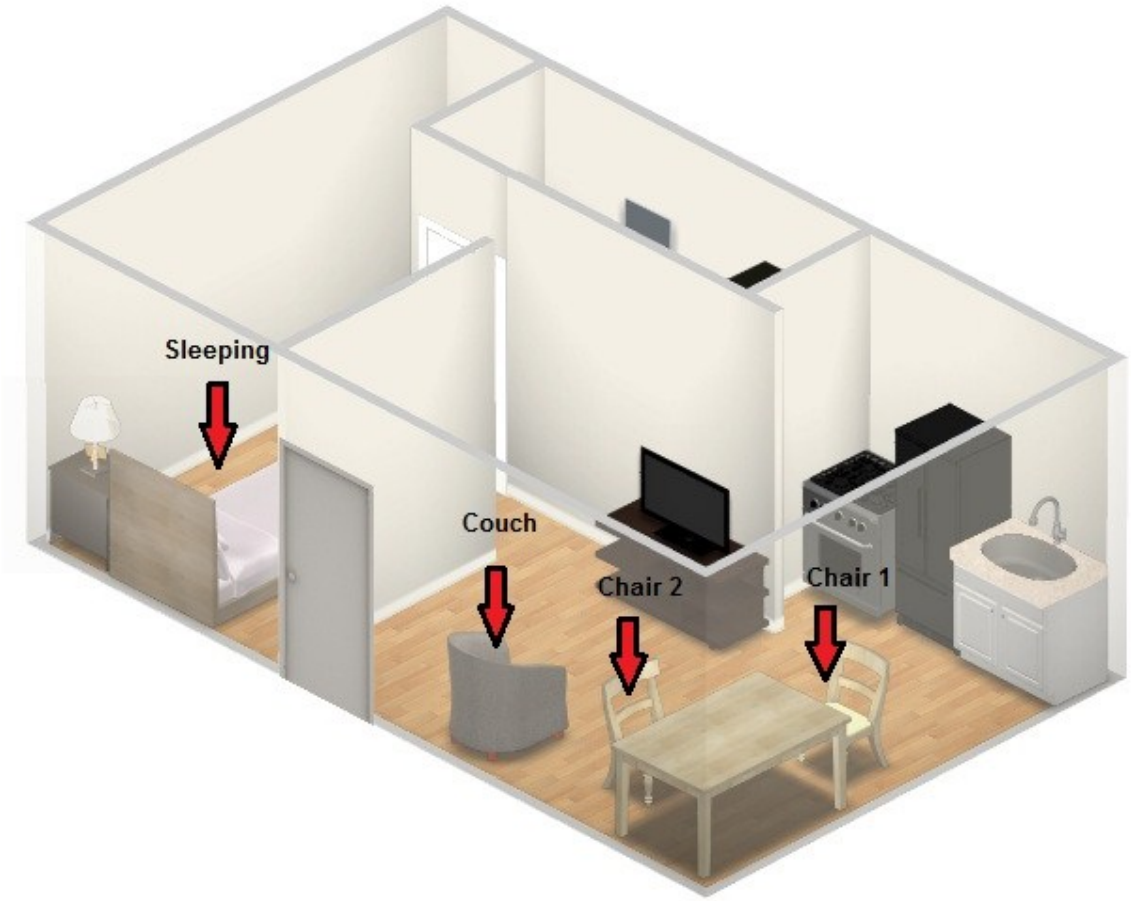

Figure 7.9 Furniture placement in mock apartment

In order to train the model to be as accurate as possible, ν parameter was varied and the false positive and false negatives was measured. Higher value of ν creates more support vectors which cover all the data complexities. Lower value of ν creates less support vectors which may not cover all the data points. Higher value of ν results in more false positives due to over training. Lower value of ν results in lower false positives but increases the false negatives.

Tables 7.7 to Table 7.10 shows the accuracy calculated for sitting and sleeping activities for different ν value.

Activity = Sitting on couch Training data = 1500 frames (2.5 minutes) Normal data = 2500 frames (≈ 4 minutes) Anomalous data = 1750 frames (≈ 3 minutes)					
ν value	Normal data Classification		Anomalous data		Average
	True Positive	Percentage Accuracy	True Negative	Percentage Accuracy	
0.03	2484	99.36%	1648	94.17%	96.77%
0.04	2484	99.36%	1618	92.46%	95.91%
0.05	2485	99.40%	1611	92.06%	95.73%
0.1	2486	99.44%	1592	90.97%	95.21%
0.25	2485	99.40%	1575	90.00%	94.70%
0.5	2485	99.40%	1562	89.26%	94.33%
0.75	2486	99.44%	1529	87.37%	93.41%
1	2486	99.44%	1527	87.26%	93.35%

Table 7.7 Sitting on couch activity recognition accuracy

Activity = Sitting on chair 1 Training data = 1500 frames (2.5 minutes) Normal data = 2500 frames (≈ 4 minutes) Anomalous data = 1750 frames (≈ 3 minutes)					
ν value	Normal data Classification		Anomalous data		Average
	True Positive	Percentage Accuracy	True Negative	Percentage Accuracy	
0.03	2490	99.60%	2454	98.16%	98.88%
0.04	2498	99.92%	2451	97.51%	98.72%
0.05	2500	100.00%	2447	97.51%	98.76%
0.1	2500	100.00%	2440	97.40%	98.70%
0.25	2500	100.00%	2436	96.53%	98.27%
0.5	2500	100.00%	2426	96.07%	98.03%
0.75	2500	100.00%	2423	95.78%	97.89%
1	2500	100.00%	2422	95.72%	97.86%

Table 7.8 Sitting on chair 1 activity recognition accuracy

Activity = Sitting on chair 2 Training data = 1500 frames (2.5 minutes) Normal data = 2500 frames (≈ 4 minutes) Anomalous data = 1750 frames (≈ 3 minutes)					
ν value	Normal data Classification		Anomalous data		Average
	True Positive	Percentage Accuracy	True Negative	Percentage Accuracy	
0.03	2431	97.24%	1750	100.00%	98.62%
0.04	2495	99.80%	1750	100.00%	99.90%
0.05	2496	99.84%	1750	100.00%	99.92%
0.1	2497	99.88%	1750	100.00%	99.94%
0.25	2500	100.00%	1750	100.00%	100.00%
0.5	2500	100.00%	1750	100.00%	100.00%
0.75	2500	100.00%	1748	99.89%	99.94%
1	2500	100.00%	1748	99.89%	99.94%

Table 7.9 Sitting on chair 2 activity recognition accuracy

Activity = Sleeping on bed Training data = 1500 frames (2.5 minutes) Normal data = 2500 frames (≈ 4 minutes) Anomalous data = 2158 frames (≈ 3 minutes)					
ν value	Normal data Classification		Anomalous data		Average
	True Positive	Percentage Accuracy	True Negative	Percentage Accuracy	
0.03	2469	98.76%	1939	89.85%	94.31%
0.04	2485	99.40%	1852	85.82%	92.61%
0.05	2492	99.68%	1785	82.72%	91.20%
0.1	2496	99.84%	1726	79.98%	89.91%
0.25	2495	99.80%	1712	79.33%	89.57%
0.5	2496	99.84%	1676	77.66%	88.75%
0.75	2496	99.84%	1726	79.98%	89.91%
1	2495	99.80%	2158	100.00%	99.90%

Table 7.10 Sleeping on bed activity recognition accuracy

In Tables 7.7 to 7.10, True positives were calculated by performing the action and measuring number of frames that were classified as the activity correctly. The true negatives were calculated by performing other activities and walking near the location of the furniture. It can be observed

that as ν value decreases false positive also reduce. For higher value of ν false positives increase due to overtraining.

The accuracy for sitting on chair 1 and sitting on chair 2 is high because these locations are closer to GridEye sensor and hence more information is received by the sensor. Comparatively sitting on couch and sleeping on bed are less accurate due to the fact that these positions are little far from sensor. Also false negatives were high in case of sleeping on bed since testing data included the person to sit on the bed. Few frames of sitting on bed were also classified falsely as sleeping on bed resulting in decrease of accuracy.

To recognize walking and standing, the total distance travelled for half sec was calculated. Human was made to walk around at normal speed of 2 feet per second. This data was recorded. Also data of human standing was also collected. The mean speed of human walking was calculated as 1.78 feet per second. Table 7.11 gives the accuracy of walking activity recognition. A threshold was used to separate walking and standing. Number of frames recognized as walking for different speeds is tabulated in Table 7.11. Normal data includes human walking around the mock apartment. Anomalous data includes human standing in a location with very slight movements.

Threshold value	Normal data Classification (3135 frames)		Anomalous data (4800 frames)		Average
Millimeter per second	True Positive	Percentage Accuracy	False Positive	Percentage Accuracy	
>200	2928	93.40%	519	89.19%	91.29%
>240	2850	90.91%	293	93.90%	92.40%
>280	2751	87.75%	169	96.48%	92.12%
>320	2620	83.57%	108	97.75%	90.66%
>360	2459	78.44%	65	98.65%	88.54%
>400	2274	72.54%	49	98.98%	85.76%
>440	2091	66.70%	35	99.27%	82.98%
>480	1866	59.52%	28	99.42%	79.47%

Table 7.11 Accuracy of Walking activity recognition

Human was made to stand still with very slight movements. The mean speed of motion when the human was standing with slight movements was measured as 0.4 feet per second. Table 7.12 gives the accuracy of standing activity recognition. Number of frames recognized as standing for different motion speeds is tabulated in Table 7.12. Normal data includes human standing in a location with very slight movements. Anomalous data includes human walking around the mock apartment.

Threshold value	Normal data Classification		Anomalous data		Average
	True Positive	Percentage Accuracy	False positive	Percentage Accuracy	
<240	4507	93.90%	285	90.91%	92.40%
<220	4416	92.00%	245	92.19%	92.09%
<200	4281	89.19%	207	93.40%	91.29%
<180	4099	85.40%	173	94.48%	89.94%
<160	3848	80.17%	136	95.66%	87.91%
<140	3488	72.67%	91	97.10%	84.88%
<120	3013	62.77%	63	97.99%	80.38%
<100	2401	50.02%	41	98.69%	74.36%
<80	1588	33.08%	28	99.11%	66.10%

Table 7.12 Accuracy of Standing activity recognition

CHAPTER X

8. CONCLUSION AND FUTURE WORK

8.1 Conclusion

In this thesis we have implemented human indoor localization and activity recognition using distributed motion sensors. We have implemented complete hardware and software setup to achieve this goal. The hardware setup includes Passive Infrared sensor node, GridEye sensor node and sink nodes. The software setup includes Arduino firmware code running on Passive Infrared sensor node and GridEye sensor node. Matlab was used to read sensor data received from the sink node. Post processing of data for localization and activity recognition was also implemented using Matlab platform. The entire setup was placed on test bed that was simulated as a mock apartment.

We have successfully implemented indoor human localization. Combination of GridEye and Passive Infrared Sensor provides human localization throughout the mock apartment. PIR sensors provide room level occupancy in kitchen and bathroom. GridEye sensors provide more accurate localization results in living room and bed room. We have implemented GridEye sensor calibration to transform the human's location in pixel coordinates to real world coordinates. Accuracy of localization was compared with ground truth values of the OptiTrack system. Average localization accuracy of less than 0.2 meters was obtained from experiments conducted on the test bed.

We have also implemented activity recognition using information obtained from the GridEye sensor. The SVM classifier is used to recognize sitting at dinning chair 1, sitting at dinning chair 2, and sitting on couch and sleeping on bed. We trained the SVM classifier with training data and later tested the classifier with testing data. Accuracy of the trained SVM model was compared by testing number of frames correctly recognized and number of false positives produced. An average accuracy of around 90% was obtained from multiple experiments conducted. An average accuracy of 90% was obtained in detecting walking and standing activities

Our thesis work provides a non-terminal based localization and activity recognition approach using distributed motion sensors. By implementing this type of sensor network, we have achieved high degree of accuracy without invading the privacy of human.

8.2 Future work

With the number of aged persons increasing drastically, Gerontechnology is gaining significance. Location information obtained from our setup could be used for various research activities involving home automation.

Currently our setup can localize a single human. Multi object tracking algorithms like particle filters could be developed to detect multiple humans. Also even though the current localization is fairly accurate, improvements can be made to further increase the accuracy. Intelligent tracking algorithms could be used to remove noise and localize more accurately.

We have implemented frame based activity recognition using SVM. Dynamic Bayesian Networks (DBNs) could be used for temporal pattern recognition. We could also experiment with different feature vectors that include temporal information to further increase the accuracy of detection.

Abundant information obtained from these sensors could be used to study behavioral and living pattern of elderly persons. This helps us to provide location based services. Air conditioner,

heaters and lighting systems could be integrated to the system to operate based on the location and activity of human.

REFERENCES

[1] World Health Organization, “10 facts on ageing and the life course”, accessed May 26, 2014, http://www.who.int/features/factfiles/ageing/ageing_facts/en/

[2] UNFPA (United Nations Population Fund); HelpAge International, “Ageing in the Twenty-First Century: A Celebration and a Challenge”, 2012

[3] Wikipedia contributors, “Elderly care”, Wikipedia, The Free Encyclopedia, http://en.wikipedia.org/wiki/Elderly_care#Promoting_independence_in_the_elderly (accessed May 19, 2014)

[4] Brian T. Horowitz, “Cyber Care: Will Robots Help the Elderly Live at Home Longer?”, *Scientific American*, Jun 21, 2010, http://www.scientificamerican.com/article/robot-elder-care/

[5] Jennifer Hicks, “Hector: Robotic Assistance for the Elderly”, Forbes, Aug 13 2012, http://www.forbes.com/sites/jenniferhicks/2012/08/13/hector-robotic-assistance-for-the-elderly/

[6] Zhang, Da, Feng Xia, Zhuo Yang, Lin Yao, and Wenhong Zhao. "Localization technologies for indoor human tracking." In *Future Information Technology (FutureTech), 2010 5th International Conference on*, pp. 1-6. IEEE, 2010.

[7] Lee, Suk, Kyoung Nam Ha, and Kyung Chang Lee. "A pyroelectric infrared sensor-based indoor location-aware system for the smart home." *Consumer Electronics, IEEE Transactions on* 52, no. 4 (2006): 1311-1317.

[8] World Economic Forum: Geneva, Switzerland, “Global Population Ageing: Peril or Promise”, http://www.weforum.org/reports/global-population-ageing-peril-or-promise.

[9] Abowd, Gregory D., Aaron F. Bobick, Irfan A. Essa, Elizabeth D. Mynatt, and Wendy A. Rogers. "The aware home: A living laboratory for technologies for successful aging." In *Proceedings of the AAAI-02 Workshop “Automation as Caregiver*, pp. 1-7. 2002.

[10] University of Florida, “The Gator Tech Smart House (GTSH)”, accessed May 26, 2014, http://www.icta.ufl.edu/gatortech/index2.html

[11] Mrazovac, B., Bjelica, M. Z., Papp, I., & Teslic, N. (2011, September). Smart audio/video playback control based on presence detection and user localization in home environment. In *Engineering of Computer Based Systems (ECBS-EERC), 2011 2nd Eastern European Regional Conference on the* (pp. 44-53). IEEE.

[12] University of Missouri. (2014, January 1). Smart America Handout. . Retrieved June 15, 2014, from http://eldertech.missouri.edu/files/MU-handout-TP-June-2014.pdf

[13] Hightower, Jeffrey, and Gaetano Borriello. "Location systems for ubiquitous computing." *Computer* 34, no. 8 (2001): 57-66.

[14] Want, Roy, Andy Hopper, Veronica Falcao, and Jonathan Gibbons. "The active badge location system." *ACM Transactions on Information Systems (TOIS)* 10, no. 1 (1992): 91-102.

[15] Ward, Andy, Alan Jones, and Andy Hopper. "A new location technique for the active office." *Personal Communications, IEEE* 4, no. 5 (1997): 42-47.

[16] Priyantha, Nissanka B., Anit Chakraborty, and Hari Balakrishnan. "The cricket location-support system." In *Proceedings of the 6th annual international conference on Mobile computing and networking*, pp. 32-43. ACM, 2000.

[17] Krumm, John, Steve Harris, Brian Meyers, Barry Brumitt, Michael Hale, and Steve Shafer. "Multi-camera multi-person tracking for easyliving." In *Visual Surveillance, 2000. Proceedings. Third IEEE International Workshop on*, pp. 3-10. IEEE, 2000.

[18] Yu, Chen-Rong, Chao-Lin Wu, Ching-Hu Lu, and Li-Chen Fu. "Human localization via multi-cameras and floor sensors in smart home." In *Systems, Man and Cybernetics, 2006. SMC'06. IEEE International Conference on*, vol. 5, pp. 3822-3827. IEEE, 2006.

[19] Hsiao, Rong-Shue, Ding-Bing Lin, Hsin-Piao Lin, Shu-Chun Cheng, and Chen-Hua Chung. "Indoor target detection and localization in pyroelectric infrared sensor networks." *IEEE VTS APWCS. Singapore City: IEEE* (2011): 115-119.

[20] Lee, Suk, Kyoung Nam Ha, and Kyung Chang Lee. "A pyroelectric infrared sensor-based indoor location-aware system for the smart home." *Consumer Electronics, IEEE Transactions on* 52, no. 4 (2006): 1311-1317.

[21] Kimata, Masafumi. "Trends in small-format infrared array sensors." In *Sensors, 2013 IEEE*, pp. 1-4. IEEE, 2013.

[22] Erickson, Varick L., Alex Beltran, Daniel A. Winkler, Niloufar P. Esfahani, John R. Lusby, and Alberto E. Cerpa. "TOSS: Thermal Occupancy Sensing System." In *Proceedings of the 5th ACM Workshop on Embedded Systems For Energy-Efficient Buildings*, pp. 1-2. ACM, 2013.

[23] Bao, L., & Intille, S. S. (2004). Activity recognition from user-annotated acceleration data. In *Pervasive computing* (pp. 1-17). Springer Berlin Heidelberg.

[24] Zhang, H., & Parker, L. E. (2011, September). 4-dimensional local spatio-temporal features for human activity recognition. In *Intelligent Robots and Systems (IROS), 2011 IEEE/RSJ International Conference on* (pp. 2044-2049). IEEE.

[25] Okada, Ryotaro, and Ikuko Yairi. "An indoor human behavior gathering system toward future support for visually impaired people." In *Proceedings of the 15th International ACM SIGACCESS Conference on Computers and Accessibility*, p. 36. ACM, 2013.

[26] Gonzalez, L. I. L., Troost, M., & Amft, O. (2013). Using a thermopile matrix sensor to recognize energy-related activities in offices. *Procedia Computer Science*, *19*, 678-685.

[27] Mathas, C., & Hearst Electronic Products (2012, August 28). *Sensing Motion with Passive Infrared (PIR) Sensors*. Retrieved March 26, 2014, from http://www.digikey.com/en/articles/techzone/2012/jun/sensing-motion-with-passive-infrared-pir-sensors

[28] LadyAda. (2014, January 18). PIR Motion Sensor. *How PIRs Work*. Retrieved May 26, 2014, from https://learn.adafruit.com/pir-passive-infrared-proximity-motion-sensor/how-pirs-work

[29] Panasonic Corporation (2012, August). *PaPIR EKMC datasheet*. Retrieved from http://www1.futureelectronics.com/doc/PANASONIC%20ELECTRIC%20WORKS/EKMC1601112.pdf

[30] Panasonic Corporation (2012, August). *PIR Motion Sensor Datasheet*. Retrieved from http://pewa.panasonic.com/assets/pcsd/catalog/papirs-ekmc-catalog.pdf

[31] Muanghlua, R., Cheirsirikul, S., & Supadech, S. (2000). The study of silicon thermopile. In *TENCON 2000. Proceedings* (Vol. 3, pp. 226-229). IEEE.

[32] Weckmann, S. (1997). *Dynamic electrothermal model of a sputtered thermopile thermal radiation detector for earth radiation budget applications* (Doctoral dissertation, Virginia Polytechnic Institute and State University).

[33] Panasonic Corporation (2012, August). *Infrared Array Sensor Grid-EYE (AMG88)*. Retrieved May 2013, from http://pewa.panasonic.com/assets/pcsd/catalog/grid-eye-catalog.pdf

[34] Autodesk Inc. (2013). Design your dream home in 3D. *Home design and decorating ideas to get inspired and get expert tips*. Retrieved May 16, 2014, from http://www.homestyler.com/

[35] Natural Point (n.d.). *OptiTrack - Flex 3 - An affordable motion capture camera*. Retrieved May 26, 2014, from https://www.naturalpoint.com/optitrack/products/flex-3/

[36] OpenCV Dev team (n.d.). *Camera calibration With OpenCV — OpenCV 2.4.9.0 documentation*. Retrieved May 2014, from http://docs.opencv.org/doc/tutorials/calib3d/camera_calibration/camera_calibration.html

[37] BootCV Contributors (n.d.). *Tutorial Camera Calibration - BoofCV*. Retrieved May 2014, from http://boofcv.org/index.php?title=Tutorial_Camera_Calibration

[38] University of Rochester Medical Center - Online Medical Encyclopedia (n.d.). *Vital Signs (Body Temperature, Pulse Rate, Respiration Rate, Blood Pressure)*. Retrieved May 2014, from http://www.urmc.rochester.edu/Encyclopedia/Content.aspx?ContentTypeID=85&ContentID=P00866

[39] Wikipedia contributors, "Room Temperature", Wikipedia, The Free Encyclopedia, http://en.wikipedia.org/wiki/Room_temperature (accessed May 19, 2014)

[40] Faragher, R. (2012). Understanding the basis of the Kalman filter via a simple and intuitive derivation. *IEEE Signal Processing Magazine*, *29*(5), 128-132.

[41] Student Dave (n.d.). *Object tracking 2D Kalman filter*. Retrieved May 2013, from http://studentdavestutorials.weebly.com/object-tracking-2d-kalman-filter.html

[42] The MathWorks, Inc. (2014). *Root-mean-square level - MATLAB rms*. Retrieved May 2014, from http://www.mathworks.com/help/signal/ref/rms.html

[43] Pollack, M. E., Brown, L., Colbry, D., McCarthy, C. E., Orosz, C., Peintner, B., ... & Tsamardinos, I. (2003). Autominder: An intelligent cognitive orthotic system for people with memory impairment. *Robotics and Autonomous Systems*, *44*(3), 273-282.

[44] Wikipedia contributors (n.d.). *Support vector machine - Wikipedia, the free encyclopedia*. Retrieved May 2014, from http://en.wikipedia.org/wiki/Support_vector_machine

[45] Fletcher, T. (2009). Support vector machines explained. *Tutorial paper., Mar*.

[46] Schölkopf, B., Williamson, R. C., Smola, A. J., Shawe-Taylor, J., & Platt, J. C. (1999). Support Vector Method for Novelty Detection. In *NIPS* (Vol. 12, pp. 582-588).

[47] Chen, P. H., Lin, C. J., & Schölkopf, B. (2005). A tutorial on ν-support vector machines. *Applied Stochastic Models in Business and Industry*, *21*(2), 111-136.

[48] The MathWorks, Inc. (2014). *Train binary support vector machine classifier - MATLAB fitcsvm*. Retrieved May 2014, from http://www.mathworks.com/help/stats/fitcsvm.html

VITA

Dharmendra Chandrashekar Kallur

Candidate for the Degree of

Master of Science

Thesis: HUMAN LOCALIZATION AND ACTIVITY RECOGNITION USING DITRIBUTED MOTION SENSORS

Major Field: Electrical Engineering

Biographical:

Education:

Completed the requirements for the Master of Science in Electrical Engineering at Oklahoma State University, Stillwater, Oklahoma in July, 2014.

Completed the requirements for the Bachelor of Engineering in your Electronics and Communication at Visvesvaraya Technological University, Belgaum, Karnataka, India in 2010.

Experience:

Worked as Graduate Teaching Assistant and Research Assistant Electrical and Computer Engineering at Oklahoma State University from January 2013 to July 2014.

Worked as Software Engineering at L&T Technology Services, Bangalore, India from October 2010 to June 2012.